SMALL SCALE STIMULI AND THE CRICKET CERCAL SYSTEM

by

Jonas L. Mulder-Rosi

A dissertation submitted in partial fulfillment
of the requirements for the degree

of

Doctor of Philosophy

in

Neuroscience

MONTANA STATE UNIVERSITY
Bozeman, Montana

January 2022

DEDICATION

To my wife Virginia, without whose support and suggestions this would not have come together. Thank you.

ACKNOWLEDGEMENTS

I would like to thank all the members of the Miller and Gray labs that I got to enjoy working alongside, with special thanks to Susan Kruger for her work in intracellular afferent staining, and Graham Cummins for his excellent visualization and spike sorting software MIEN (https://github.com/gic888/MIEN). I would like to thank Charley Gray, Steve Stowers, Tomas Gideon, and Dan Barth for their time and excellent questions that have helped resurrect this thesis. And I would like to offer a special “thank you” to John Miller for his energy and passion for an ever deeper understanding of coding generally and the cercal system particularly, stating from first understanding interneuron tuning and running unabatedly through the work presented here.

This work was partially funded by a generous Kopriva Graduate Student Fellowship from the Kopriva Foundation.

TABLE OF CONTENTS

TABLE OF CONTENTS CONTINUED

LIST OF FIGURES

Figure Page

ABSTRACT

The cricket cercal system has been a model system in neuroscience for over 30 years. Anatomy, physiology, and theory have all come together to produce a picture of a system with a clear purpose: encoding air direction around the animal. However, certain features of the system have suggested that these cells may be sensitive to additional stimulus dimensions.

To address this limited stimulus space I designed new experiments to test these neurons' responses to previously untested stimuli. I used a novel extracellular recording mechanism able to record and sort several neurons' responses at the same time. I built and tested several stimulators to provide small-scale puffs to specific parts of the sensory array at specific times. With these, I was able to test this model neural system against a complex stimulus space.

I show here that these neurons respond to several additional stimulus dimensions. They are tuned to the timing of stimuli across the array. They show differential responses to even more complex stimuli with varying stimulus directions in different locations across the array.

This implies that the previous understanding of the system was likely limited by how it was tested. While these cells accurately encode the direction of large-scale airflow, they also encode other aspects of stimuli, such stimulus timing and small-scale variations in stimulus direction. Thus the "function" of these neurons may be far more complex than previously understood.

CHAPTER ONE

INTRODUCTION

The cercal sensory array of the cricket is a mechanosensory system that encodes information about the direction and dynamic properties of low-velocity air currents (Jacobs et al., 2008). The sense organ for this system consists of a pair of antenna-like abdominal appendages called cerci, each of which is ~1-cm long in normal adult crickets and covered with ~750 wind-sensitive filiform hairs (Miller et al., 2011). Within the terminal abdominal ganglion (TAG), the sensory afferents make excitatory synapses onto a population of ~100 local and projecting interneurons (INs). On the basis of the information conveyed by approximately 20 of these projecting INs, the animal must determine stimulus source direction and discriminate between different possible signal sources with few false classifications (Gnatzy and Heusslein, 1986).

Analogous cercal systems are present in most Orthoptera. It is remarkable, nonetheless, that other species make do with very small cerci (Figure 1). Although the cercal sensory system of the cricket has been the subject of anatomical, developmental, functional and theoretical research over the last four decades, the functional significance of the spatial extent of the cricket's sensory array due to these elongated cerci has not been assessed in depth.

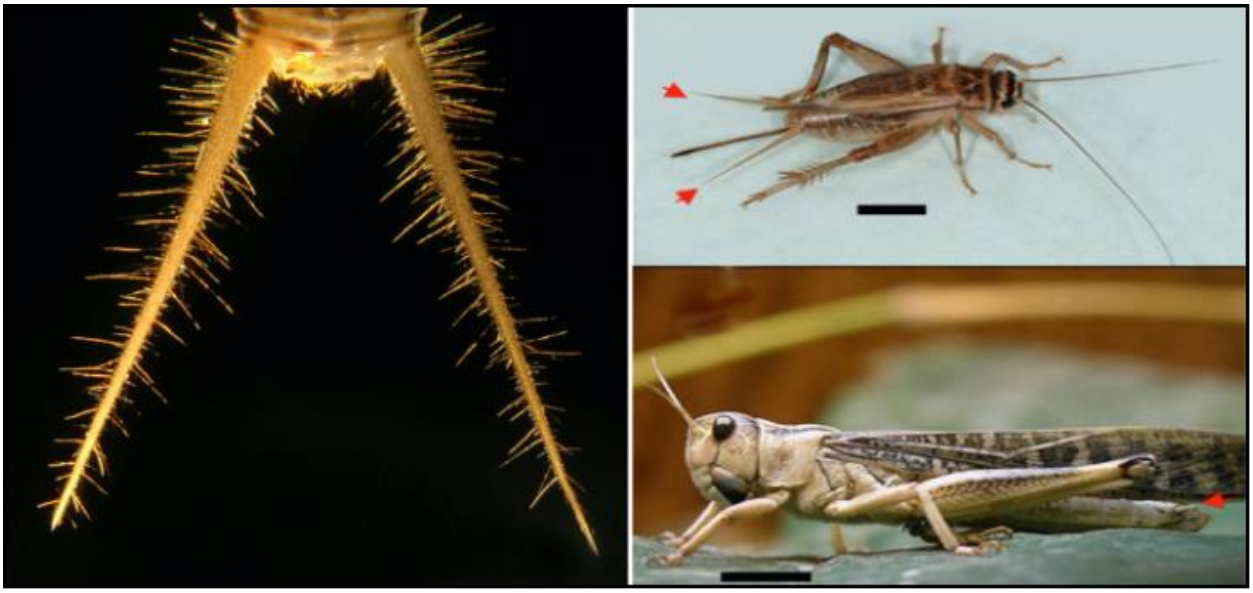

Figure 1.1. The cercal sensory array of the cricket. The left panel shows a top-down view of a cricket's two cerci covered in wind-sensitive filiform hairs. The right panel shows the relative sizes of the cercal array in crickets (top) and locusts (bottom) with 5-mm scale bars.

All but a few of the large body of neurophysiological and theoretical studies of the cercal sensory system have been based on experiments using bulk flow air current stimuli, *i.e.*, stimuli that simultaneously deflect all filiform mechanosensory hairs along the entire length of both cerci. One set of four cercal INs that receive input from the filiform mechanosensory array has been the focus of a great many studies using these bulk-flow stimuli: INs Left 10-2, Right 10-2, Left 10-3 and Right 10-3 (Jacobs and Murphey, 1987). Hypotheses for the behavioral role, functional organization and ensemble neural coding scheme of this four-cell ensemble have been proposed based on bulk-flow stimulus-response experimental paradigms. Specifically, these four INs have been shown to be tuned broadly to stimulus direction and velocity (Figure 2). It is thought that this subsystem operates by projecting a coarse-coded image of these parameters to higher centers, where sophisticated feature detectors operate on this information (Figure 3) (Butts and Goldman, 2006; Miller et al., 1991; Salinas and Abbott, 1994; Theunissen et al.,

1996; Theunissen and Miller, 1991). This has become a textbook example of neural coding where a stimulus dimension (direction of bulk airflow) is encoded by a set of neurons. Additionally, the morphology of the cells seems to effectively explain their tuning (Miller and Jacobs, 1984). This is often seen as implying that the biological function of these neurons is fully understood.

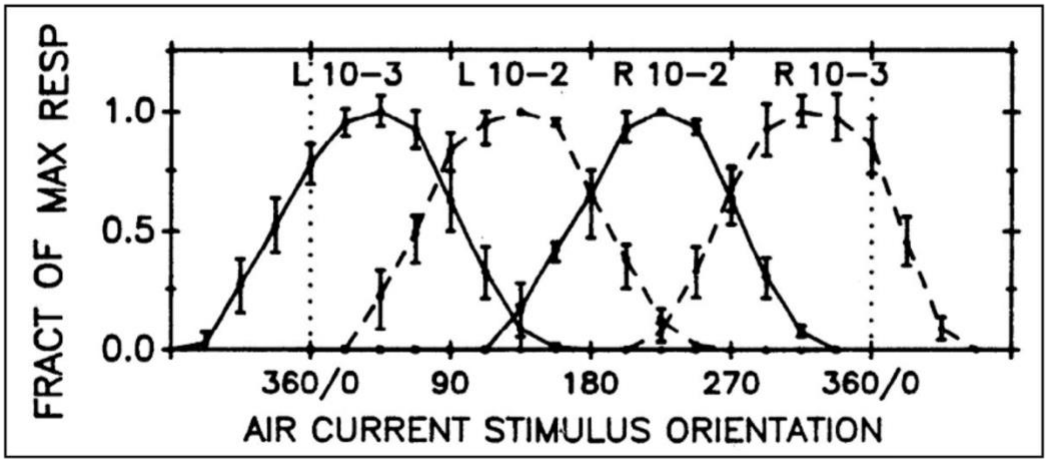

Figure 1.2. Overlapping directional tuning curves of INs 10-2 and 10-3. This figure (modified from Miller et al., 1991) shows half-cosine like directional tuning curves for the complete set of bilaterally symmetric left (L) and right (R)10-2 and 10-3 INs. The ordinate shows the direction from which air motion proceeds in degrees, with 0 corresponding to bulk airflow coming from directly in front of the animal. Abscissa values are normalized firing rate. These four INs effectively cover all cardinal directions and thus differentially encode the direction of bulk airflow.

Large-scale bulk airflow stimuli like those used in previous experiments occur naturally during the animal's own self-movement or as typical large-scale background noise in the environment. However, many behaviorally relevant air-current stimuli would be expected to be very different from the bulk-flow stimuli used in most previous neurophysiological experiments. Examples of such stimuli include small recirculating vortex-like stimuli that would impose different directional forcing vectors simultaneously and/or sequentially at different positions along the cerci (Heinzel and Dambach, 1987; Kamper and Dambach, 1981), and discrete air

current wavefronts that sweep along the cerci (Casas et al., 2008; Comer et al., 1994; Gnatzy and Heusslein, 1986; Gnatzy and Kamper, 1990; Magal et al., 2006). Over the last few years, Casas, Dangles and colleagues have characterized the small-scale spatiotemporal structure of the dynamic air currents generated by predatory spiders during attacks on crickets, and have also demonstrated the importance of using behaviorally-relevant stimuli in neuroethological studies (Casas et al., 2008; Casas and Dangles, 2010; Casas and Steinmann, 2014; Dangles et al., 2009, 2006; Dupuy et al., 2012; Magal et al., 2006; Steinmann and Casas, 2017). Further, it has been shown recently in another type of insect mechanosensory system that the dynamic response of action potential encoding is different for naturalistic stimuli *vs.* the white noise stimuli used in many of the earlier experiments designed to study cricket cercal system encoding (Pfeiffer and French, 2015). By limiting the stimuli used to test cercal INs, it is possible that only a partial understanding of these cell's function has been obtained. Current understanding likely fits in a far larger context of stimulus selectivity including responsiveness to small-scale dynamics. The primary goal of this dissertation is to use complex, behaviorally relevant stimulus-space parameters to test investigate the importance of small-scale stimulus dynamics in driving the firing of the 10-2/10-3 neuronal ensemble. Results challenge current IN paradigms, both explaining previously unintelligible information and suggesting improvements to the current models.

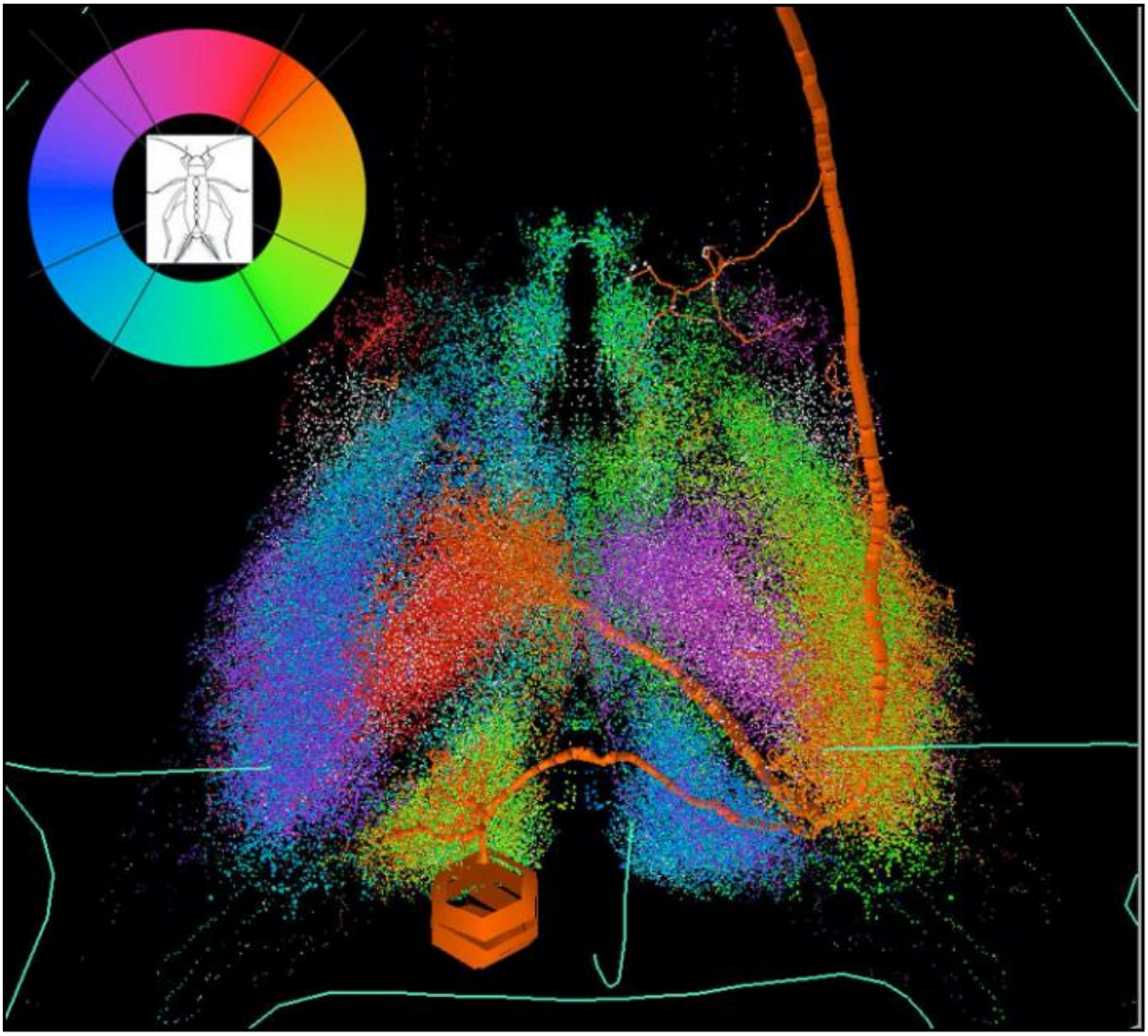

Figure 1.3. A model of 10-3 in the afferent map. Left IN 10-3 is shown in orange embedded in the color-coded afferent map. Stippled colors correspond to the most likely directional response of afferents whose axons occur in a given location area of the terminal abdominal ganglia. The inset color wheel shows the correspondence between map colors and the direction of airflow around the animal. For instance, afferents synapsing in a purple region of the map would respond to air motion coming from the left-front of the animal. The turquoise outline shows the boundaries of the terminal abdominal ganglion.

In Chapter 2, I describe the use of a novel stimulating apparatus capable of sequentially exciting small patches of hairs along the cercus to produce temporally complex multi-directional air movements having spatial resolution finer than the scale of the cercal array. Experiments

performed with this apparatus allowed me to evaluate the extent to which the distribution of receptor hairs out along the length of the cerci leads to temporal dispersion of the receptors' spike trains on entry into the terminal abdominal ganglion. The observed dispersion and its functional significance are presented in this chapter.

To assess the optimal stimulus space for the IN group of 10-2 and 10-3 in response to small-scale stimulus, I paired the stimuli with simultaneous recordings from most of the projecting giant INs. I then built highly accurate 3D models of these INs using synaptic connectivity and active channel data and used them to predict the responsiveness of INs 10-2a and 10-3a to a wide range of fine-grained air-motion stimuli. These predictions were then tested *in vivo*, providing a tuning surface in complex spatiotemporal stimulus space that includes the previously observed functionality of these cells. I discuss the methods, results, and conclusions of these experiments in Chapter 3.

Finally, Chapter 4 provides an integrated view of the cricket's cercal sensory system. I discuss how information on the effects of small-scale dynamics moves forward our understanding of this model system and serves as a good test of how much we can learn about neuronal function from easily observed neuronal anatomy. This work was supported by NIH/NSF grant CRCNS-0515290, NSF grant CMMI-0849433, and NSF grant EF-0425878.

References

Butts, D.A., Goldman, M.S., 2006. Tuning curves, neuronal variability, and sensory coding. PLoS Biol 4, e92. https://doi.org/10.1371/journal.pbio.0040092

Casas, J., Dangles, O., 2010. Physical Ecology of Fluid Flow Sensing in Arthropods. Annu. Rev. Entomol. 55, 505–520. https://doi.org/10.1146/annurev-ento-112408-085342

Casas, J., Steinmann, T., 2014. Predator-induced flow disturbances alert prey, from the onset of an attack. Proc. R. Soc. B. 281, 20141083. https://doi.org/10.1098/rspb.2014.1083

Casas, J., Steinmann, T., Dangles, O., 2008. The aerodynamic signature of running spiders. PLoS ONE 3, e2116. https://doi.org/10.1371/journal.pone.0002116

Comer, C., Mara, E., Murphey, K., Getman, M., Mungy, M., 1994. Multisensory control of escape in the cockroach Periplaneta americana. Journal of Comparative Physiology A 174, 13–26.

Dangles, O., Irschick, D., Chittka, L., Casas, J., 2009. Variability in sensory ecology: expanding the bridge between physiology and evolutionary biology. The Quarterly Review of Biology 84, 51–74. https://doi.org/10.1086/596463

Dangles, O., Ory, N., Steinmann, T., Christides, J.-P., Casas, J., 2006. Spider's attack versus cricket's escape: velocity modes determine success. Animal Behaviour 72, 603–610. https://doi.org/10.1016/j.anbehav.2005.11.018

Dupuy, F., Steinmann, T., Pierre, D., Christidès, J.-P., Cummins, G., Lazzari, C., Miller, J., Casas, J., 2012. Responses of cricket cercal interneurons to realistic naturalistic stimuli in the field. Journal of Experimental Biology 215, 2382–2389. https://doi.org/10.1242/jeb.067405

Gnatzy, W., Heusslein, R., 1986. Digger wasp against crickets: I. Receptors involved in the antipredator strategies of the prey. Naturwissenschaften 73, 212–215. https://doi.org/10.1007/BF00417728

Gnatzy, W., Kamper, G., 1990. Digger wasp against crickets. II. An airborne signal produced by a running predator. J Comp Physiol A 167. https://doi.org/10.1007/BF00190826

Heinzel, H.-G., Dambach, M., 1987. Travelling air vortex rings as potential communication signals in a cricket. J. Comp. Physiol. 160, 79–88. https://doi.org/10.1007/BF00613443

Jacobs, G.A., Miller, J.P., Aldworth, Z., 2008. Computational mechanisms of mechanosensory processing in the cricket. Journal of Experimental Biology 211, 1819–1828. https://doi.org/10.1242/jeb.016402

Jacobs, G.A., Murphey, R.K., 1987. Segmental origins of the cricket giant interneuron system. J. Comp. Neurol. 265, 145–157. https://doi.org/10.1002/cne.902650110

Kamper, G., Dambach, M., 1981. Response of the cercus-to-giant interneuron system in crickets to species-specific song. J. Comp. Physiol. 141, 311–317. https://doi.org/10.1007/BF00609933

Magal, C., Dangles, O., Caparroy, P., Casas, J., 2006. Hair canopy of cricket sensory system tuned to predator signals. Journal of Theoretical Biology 241, 459–466. https://doi.org/10.1016/j.jtbi.2005.12.009

Miller, J.P., Jacobs, G.A., 1984. Relationships between neuronal structure and function. J Exp Biol 112, 129–145.

Miller, J.P., Jacobs, G.A., Theunissen, F.E., 1991. Representation of sensory information in the cricket cercal sensory system. I. Response properties of the primary interneurons. Journal of Neurophysiology 66, 1680–1689. https://doi.org/10.1152/jn.1991.66.5.1680

Miller, J.P., Krueger, S., Heys, J.J., Gedeon, T., 2011. Quantitative characterization of the filiform mechanosensory hair array on the cricket cercus. PLoS ONE 6, e27873. https://doi.org/10.1371/journal.pone.0027873

Pfeiffer, K., French, A.S., 2015. Naturalistic stimulation changes the dynamic response of action potential encoding in a mechanoreceptor. Front. Physiol. 6. https://doi.org/10.3389/fphys.2015.00303

Salinas, E., Abbott, L.F., 1994. Vector reconstruction from firing rates. J Comput Neurosci 1, 89–107. https://doi.org/10.1007/BF00962720

Steinmann, T., Casas, J., 2017. The morphological heterogeneity of cricket flow-sensing hairs conveys the complex flow signature of predator attacks. J. R. Soc. Interface. 14, 20170324. https://doi.org/10.1098/rsif.2017.0324

Theunissen, F., Roddey, J.C., Stufflebeam, S., Clague, H., Miller, J.P., 1996. Information theoretic analysis of dynamical encoding by four identified primary sensory interneurons in the cricket cercal system. Journal of Neurophysiology 75, 1345–1364. https://doi.org/10.1152/jn.1996.75.4.1345

Theunissen, F.E., Miller, J.P., 1991. Representation of sensory information in the cricket cercal sensory system. II. Information theoretic calculation of system accuracy and optimal tuning-curve widths of four primary interneurons. Journal of Neurophysiology 66, 1690–1703. https://doi.org/10.1152/jn.1991.66.5.1690

CHAPTER TWO

THE CRICKET CERCAL SYSTEM IMPLEMENTS DELAY-LINE PROCESSING

Contribution of Authors and Co-Authors

Manuscript in Chapter 2

Author: Jonas L. Mulder-Rosi

Contributions: Designed study, carried out experiments, analyzed data, and wrote the manuscript

Co-Author: Graham I. Cummins

Contributions: Designed visualization and analysis software framework

Co-Author: John P. Miller

Contributions: Obtained funding, designed study, discussed ideas, and edited the manuscript

Manuscript Information

Jonas L. Mulder-Rosi, Graham I. Cummins, John P. Miller

Journal of Neurophysiology

Status of Manuscript:
____ Prepared for submission to a peer-reviewed journal
____ Officially submitted to a peer-reviewed journal
____ Accepted by a peer-reviewed journal
_x__ Published in a peer-reviewed journal

American Physiological Society
Issue 103(4)
DOI: 10.1152/jn.00875.2009

CHAPTER TWO

THE CRICKET CERCAL SYSTEM IMPLEMENTS DELAY-LINE PROCESSING

Introduction

The cercal sensory system of the cricket functions as a low-frequency, near-field extension of the animal's auditory system, and encodes information about the direction and dynamic properties of low-velocity air currents with great accuracy and precision. This system has been shown to be of critical importance for a variety of behaviors, from oriented escape responses to mate location (Jacobs et al., 2008).The sense organ for this system consists of a pair of antenna-like appendages called cerci at the rear of the cricket's abdomen. In *Acheta domesticus*, each cercus is approximately 1cm long in a normal adult cricket and is covered with approximately 750 filiform mechanosensory hairs (Palka et al., 1977). Different filiform hairs have different directional and frequency sensitivities, which are determined by the structure, length and location of the hairs on the cercus (Edwards and Palka, 1974; Landolfa and Jacobs, 1995; Shimozawa and Kanou, 1984). Each hair is innervated by a single spike-generating mechanosensory receptor neuron (Edwards and Palka, 1974), and the afferent axons of the entire ensemble of hairs project into the terminal abdominal ganglion (TAG) to form a continuous internal representation of air current parameters (Bacon and Murphey, 1984; Jacobs and Theunissen, 1996). The goals of our study were to determine if the distribution of receptor hairs out along the length of the cerci leads to temporal dispersion of the receptors' spike trains upon entry into the TAG, and to investigate the functional significance of any observed dispersion.

The cercal system has been the subject of many anatomical, developmental, functional and theoretical studies over the last 35 years. All but a few of the neurophysiological and theoretical studies have been based on experiments using "bulk flow" air current stimuli, *i.e.*, stimuli that simultaneously activate all filiform hairs along the entire length of the cerci. Such experimental stimuli are typically generated by the movement of loudspeaker cones placed in close proximity to the specimens: movement of the speakers results in the displacement of a block of air around the cricket's cerci that is much larger than the scale of the cerci themselves. Large-scale bulk air flow would occur naturally during the animal's own self-movement or as typical background "noise" in the environment. However, many (perhaps most) behaviorally-relevant stimuli would be expected to have spatial structure at a smaller scale than the characteristic scale of the cerci. Examples of such stimuli include discrete air current wavefronts that sweep along the cerci (Comer et al., 1994; Gnatzy and Heusslein, 1986; Gnatzy and Kamper, 1990; Magal et al., 2006), and small recirculating vortex-like stimuli that would impose different directional forcing vectors simultaneously and/or sequentially at different positions along the cerci (Heinzel and Dambach, 1987; Kamper and Dambach, 1981). Studies by Casas, Dangles and colleagues over the last few years have characterized, with great accuracy and precision, the small-scale spatiotemporal structure of the dynamic air currents generated by predatory spiders during attacks on crickets, and have also demonstrated the importance of using behaviorally-relevant stimuli in neuroethological studies (Casas et al., 2008; Dangles et al., 2009, 2006; Magal et al., 2006).

Despite the recognized importance of using ethologically relevant stimuli, to the best of our knowledge none of the theoretical or modeling studies of the cercal system interneuron

stimulus-response properties have taken differential conduction delay along the cercus into account and may therefore have significantly misinterpreted the response characteristics of the cercal interneurons. To illustrate the problem, consider the effects of two different air current stimuli on the distribution of synaptic inputs from the array of cercal sensory afferents onto the primary cercal interneurons. The first stimulus, equivalent to that used in all previous publications from our research group (and several other groups), is the simultaneous activation of all cercal filiform hairs with bulk airflow. If the spikes generated by distal receptors arrive at the TAG at a significant lag with respect to spikes from the proximal hairs, then a brief impulsive bulk air current stimulus would manifest as a temporally dispersed distribution of synaptic inputs onto the dendrites of a cercal interneuron. In contrast, consider the effect of a second type of air current stimuli: an air current wavefront that sweeps along the cercus from tip to base at a speed equivalent to the propagation speed of the afferent spikes. The movement of the waveform would be expected to "deblur" the temporal dispersion of the ensemble afferent response and would yield a summed temporal distribution of synaptic inputs onto interneuron dendrites that was narrower in time and larger in amplitude.

The first goal of the studies reported here was to determine if there is any differential propagation time for spikes from filiform receptors at different locations along the length of a typical adult cercus. The second goal is to determine the functional significance of the extended distribution of filiform receptors, as judged by observing the differential responses of primary sensory interneurons to simultaneous *vs.* sequential activation of the cercal filiform receptor array. As we will demonstrate, the differential conduction characteristics of the filiform receptor array are, in fact, of substantial significance. All filiform afferent axons have the same

propagation speeds to within a very small variance, resulting in a significant dispersion of the spikes generated by bulk air movements. Using an air current stimulus device capable of generating sequences of air jets along a single cercus, we demonstrate that the cerci operate as delay-lines and support neural computations in many of the projecting cercal interneurons (INs) that yield substantial differential sensitivity to the direction and velocity of these more complex stimuli. We demonstrate that several cercal INs show much greater sensitivity to stimuli that sweep along the cerci than they do to bulk air-flow stimuli, functioning as "notch filters" with selective insensitivity to bulk-flow stimuli.

Materials and Methods

Dissection, Specimen Preparation, and Electrophysiological Recording

All experiments were performed on adult female *Acheta domesticus* crickets, obtained from Bassett's Cricket Ranch (Visalia, CA). Each cricket specimen was selected within four hours following the final molt and anesthetized by placement on ice until it ceased to show escape behavior when touched. The legs and wings were removed. Subsequent stages of the specimen preparation depended upon the specific experimental protocols to be used. All recordings were made at room temperature.

Measurement of Sensory Afferent Axonal Conduction Times. Measurements of filiform afferent spike propagation speed required simultaneous recordings of afferent spikes at two different locations: one out along a cercus, and one from the cercal nerve at the base of the cercus. For these experiments, a 3 mm x 8 mm section of dorsal cuticle was removed. Digestive, reproductive, and superficial fat tissues were removed along with the ovipositor. The abdominal

cavity was filled with isotonic saline solution (O'Shea and Adams, 1981), and perfused periodically. The preparation was pinned to a plate of silicone elastomer. To achieve mechanical stability for durations of up to two hours, movements of the cerci were constrained by gluing each cercus to the silicone elastomer with marine epoxy. The entire plate-mounted preparation was placed on a vibration isolation table in a laminar air-current chamber. A set of filiform hairs to be studied was identified using a stereo dissecting microscope, and the surrounding hairs were plucked out with fine forceps to provide access for the placement of tungsten electrodes and to reduce extraneous action potentials from nearby hairs. For control purposes, several measurements were taken from animals without plucking hairs and without epoxy applications to the distal cercus. Measurements from these animals were statistically indistinguishable from those taken with the standard protocols described above. Data from these control measurements were included in the subsequent analysis.

To record from sensory afferent axons in the cercus, two matched-impedance tungsten electrodes (FHC Inc., Bowdingham ME) were used: one as the recording electrode and one as the indifferent electrode. The tip of the recording electrode was inserted just below the cuticle and just proximal to the base of a filiform hair. The indifferent electrode was placed on the cuticle a small distance from the recording electrode. The two electrodes were attached to the inputs of a differential amplifier (Data, Inc., Model 2124) and signals were amplified at a gain of 300-1800x and bandpassed between 100 and 10,000 Hz.

To achieve simultaneous recordings from the same afferent axons in the cercal nerve, ensemble spiking activity through the entire cercal nerve was recorded near its exit point from the cercus using a glass suction electrode in the *en passant* configuration. The electrode was

filled with standard isotonic saline and isolated from the intra-abdominal bath with petroleum jelly. The suction electrode was connected to a differential amplifier (Data, Inc., Model 2124) grounded to the abdominal saline bath. Signals were amplified at 300x and bandpassed between 100 and 10,000 Hz.

Spikes recorded from the tungsten pair were used for spike-triggered averaging of activity through the cercal nerve suction electrode recordings. The averaging was carried out off-line after the experiment, using custom software based on Matlab v7.3. For the experiments requiring calculation of the spike propagation times, variation in proximal electrode placement and cercal nerve stretch was corrected for by removing the ordinate intercept value from each animal such that a hair 0 mm from the base would show 0 ms of latency.

Recording from Sensory Interneuron Axons in the Abdominal Nerve Cord. Some experiments required multi-channel, multi-unit extracellular recordings from the abdominal nerve cord between the terminal abdominal ganglion and the thoracic ganglia. To enable these recordings, the preparation was dissected beyond the minimal levels described above. After removal of the head as well as digestive, reproductive and superficial fat tissues from the abdominal cavity, the specimen was pinned out on silicone elastomer. The entire nerve cord was then surgically isolated from all connections to the remainder of the body by cutting all peripheral nerves, trachea, and connective tissue between the terminal abdominal ganglion and the prothoracic ganglion. All of the animal's body was cut away and discarded except for the abdominal nerve cord including all thoracic ganglia, all abdominal ganglia, the cercal nerves, the body walls of the posterior half of the abdomen (split along the dorsal and ventral midlines to the

level of the cuticular cap at the posterior end of the abdomen), and the two cerci with all sensory hairs intact.

For a subset of these experiments, we reduced the filiform mechanosensor array by plucking out all of the filiform hairs on a cercus except those on the lateral and medial sides. This procedure eliminated all hairs that were activated by air currents oriented transversely or obliquely to the long axis of the cercus, leaving only those hairs activated by air currents directly in line with the cercus. This procedure was done to control for the possibility that turbulence surrounding the air jets generated by the air current nozzles was resulting in variable activation of transverse hairs, thus confounding interpretation of the stimulus-response variability. IN stimulus-response characteristics from preparations having these reduced sensory arrays yielded results that were qualitatively and quantitatively similar to those obtained from preparations with full, unmodified sensory arrays.

The reduced preparation was transferred to a specially constructed platform and perfused periodically with isotonic saline. The platform was constructed to have a physical profile approximating the body shape of an adult cricket, and enabled placement of the two cerci in a manner that was equivalent to their configuration on a freely-behaving animal, *i.e.*, elevated at 15° from the horizontal plane and at an angular separation of 60° (Landolfa and Jacobs, 1995). A mounted preparation is shown in Figure 1A. After the preparation was stabilized on the perfusion platform, the right connective of the abdominal nerve cord was cut at a point midway between the terminal ganglion and next-most anterior ganglion. This left only the projecting axons in the left connective intact, which greatly simplified the subsequent tasks of cell identification and analysis from the multi-unit recordings.

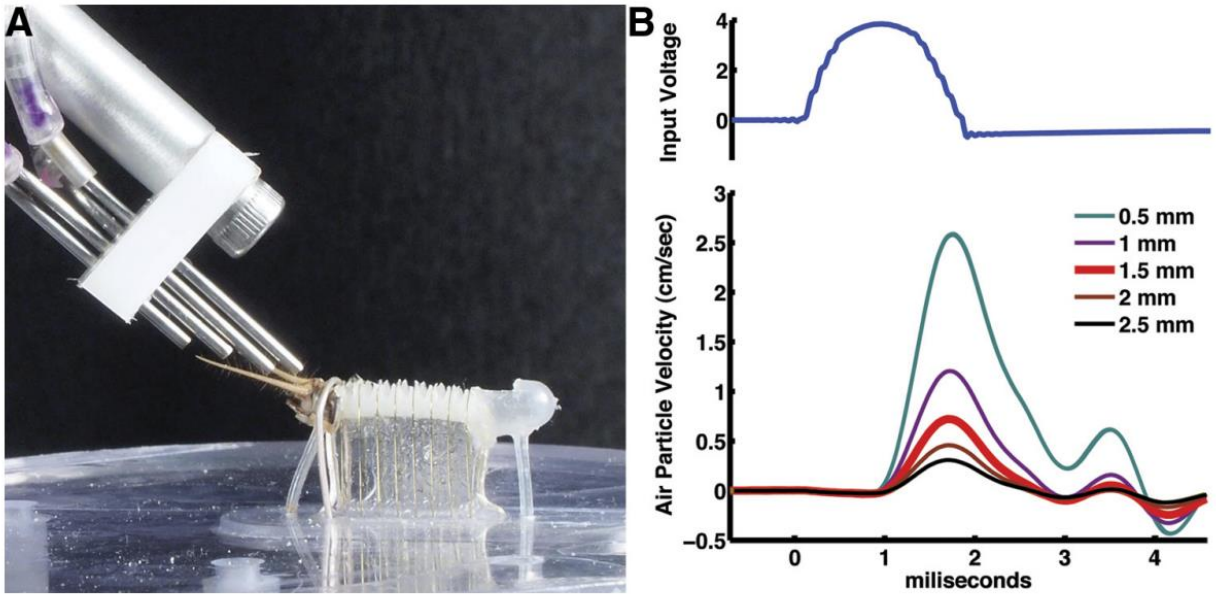

Figure 2.1. Multi-nozzle air-current stimulus device. A. Photograph of the multi-nozzle stimulus device, positioned over a cricket cercus as in the actual experimental preparations. B. Plot of the air currents generated through a single nozzle, recorded with the MicroFlown positioned at five different distances from the nozzle tip. The top trace is the voltage signal sent to the mini-speaker connected to the nozzle, and the bottom five traces are plots of air current velocity vs. time at the different indicated distances between the nozzle tip and MicroFlown sensor.

The array of extracellular electrodes consisted of a set of eight insulated stainless-steel wires (California Fine Wire Co., 0.005in HML coated) integrated into the preparation chamber, and a ninth un-insulated silver wire that served as a common (grounded) reference electrode. These eight wires were placed across the top of the preparation chamber, perpendicular to the long ("body") axis, at an inter-wire spacing of approximately 1 mm. Each of the eight transverse wires had a small patch of the HML insulator removed along the center axis of the chamber, to function as the point of electrical contact with the abdominal nerve cord. At the beginning of each experiment, the nerve cord was positioned to extend across the un-insulated patches of the eight-electrode array and shielded from the bath with a mixture of 70% petroleum jelly and 30% mineral oil. The right hemi-connective was then cut between the terminal ganglion and the next

most anterior ganglion, so that the axons from only 10 of the 20 projecting interneurons were recorded. The entire preparation was placed into a laminar air-current chamber on a vibration isolation table. The leads from the eight electrodes and common reference electrode were attached to a bank of differential amplifiers constructed in our lab, and signals were amplified at a gain of 1000-2000x and bandpassed between 100 and 10,000 Hz.

Spike trains from all eight recording electrodes, plus records of all stimulus waveform channels, were digitally sampled at 40 kHz (DataMAX, R.C. Electronics Inc., Santa Barbara CA) and stored for subsequent analysis. Signals were also monitored simultaneously on a digital oscilloscope. Spike discrimination was accomplished using the phased-array spike discrimination technique described in detail elsewhere (Huang and Miller, 2004), as implemented in the general-purpose data analysis program suite MIEN *http://mien.msu.montana.edu/*.

Air Current Stimulus Generation

A device was used to generate independent air current jets at four different positions along a single cercus. The device is shown in Figure 1A and consisted of four small-diameter stainless steel nozzles (1-inch lengths of 18-gauge hypodermic syringe needles) connected to a corresponding set of four micro-speakers of the type used in headphones (Radio Shack 273092), via 3-inch lengths of small-diameter tygon tubing. Movement of a single micro-speaker cone drove air through the corresponding nozzle. Coordinated control of the four micro-speakers with a 4-channel computer-controlled signal generator (National Instruments) enabled the generation of arbitrarily complex sequences of air currents through the four nozzles. For each experiment, the tips of the four tubes were adjusted to direct air currents at four equally spaced positions along a single cercus, from a distance of 1.5 mm above the cercus.

For the experiments we report here, the individual stimulus waveforms sent to each speaker were unidirectional jets. The waveform of each jet was constructed to present approximately a half cosine wave (*i.e.*, a positive-velocity air displacement with no discontinuities at the beginning and termination). Air velocities and waveforms were measured using a low-velocity air current sensor (MicroFlown Technologies, Titan sensor, Zevenaar, Netherlands), placed 1.5 mm from the nozzle. Example measurements are shown in Figure 1B and confirmed that the half-period cosine wave produced primarily an outward going "puff" without significant rebounding airflow. For all experiments shown here, the peak velocity of the air puffs was set to values measured to be in the range from 2 to 7 mm/sec at the target location on the cercus. The MicroFlown was used to verify that the air current velocity fell to below 10% of the peak velocity at a distance away from the axis of the nozzle equal to the inter-nozzle spacing. Single filiform hairs may be excited by air current velocities below 10% of the velocity at the target location. However, when producing only these low velocity air currents no alteration in the behavior of either the cercal nerve or the projecting interneurons could be measured. Visual inspection under the microscope supported the functional irrelevance of low velocity air currents: during a single puff from an individual nozzle, only the filiform hairs directly below the center of the nozzle could be seen to move, and there was no perceptible movement of any hairs at a distance greater than the diameter of the nozzle.

Three different classes of puff sequences were used. The first class was a control stimulus, in which all four positions along the cercus were activated simultaneously. This set was equivalent to a uniform bulk air displacement, similar to those that have been used in all previous studies that used standard loudspeakers to generate bulk airflow over an entire cricket specimen.

The second stimulus class was a sequence that started at the tip of a cercus and swept toward the base of the cercus. The third class was a sequence that swept in the opposite direction: from base to tip. The speed of the moving sequences was varied by changing the intervals between the individual puffs. For the experiments reported here stimuli were presented every 500 ms with the direction and velocity of sweep randomized.

We note that the nozzles were positioned and aligned with the cercus in a manner that resulted primarily in the deflection of the "longitudinal" hairs, *i.e.*, those hairs located on the lateral and medial aspects of the cercus that have movement axes in line with the long axis of the cercus. The "transverse" hairs located on the dorsal and ventral aspects of the cercus have movement axes that were perpendicular to the direction of the air jets, and when present were minimally activated by the jets (as determined by visual inspection).

Results

Spike Conduction Latencies for Sensory Afferent Axons in the Cerci

We measured the action potential conduction speeds for a sample of twenty-three sensory afferents from filiform mechanosensory hairs on cerci from six different crickets. The filiform hairs innervated by this sample of afferents were located on the dorsal cercal surface, had movement axes that were perpendicular to the cercal axis, and ranged in length from 500 to 1200 μm. For each hair we studied, simultaneous recordings at two different sites were obtained from the sensory afferent axon that innervated the hair. The first recording site was on the cercal nerve at the base of the cercus, and the second recording site was out along the cercus, at a distance from the base that ranged from approximately 15% to 80% of the entire cercal length for the

different hairs in our sample set. For each hair we studied, the distance between the distal recording site and the base of the cercus was measured from a digital micrograph taken through a stereo dissecting microscope during the experiment. Figure 2 shows a typical dataset from a single filiform afferent, resulting from spike-triggered averaging of approximately 1000 samples. The top trace is an average of the largest unit recorded from the tungsten electrode at the base of the hair. The individual spikes recorded at this tungsten electrode were used as the trigger for averaging the activity recorded through the suction electrode at the base of the cercus, shown in the lower trace. The propagation time was measured as the time between the peak in the distal trace and the first peak in the averaged proximal traces. Later peaks in the proximal trace were found not to respond to air current stimuli and were ignored. These later peaks were due, presumably, to activity of the hairs in response to the un-controlled background air currents in the experimental chamber, and/or to subsequent spikes elicited by rebound of the hairs to the air current stimuli.

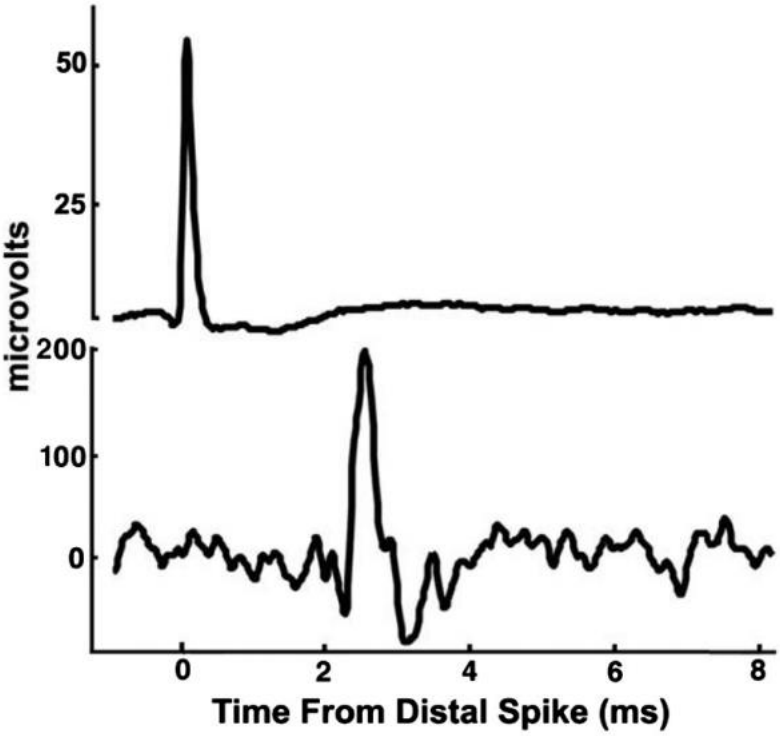

Figure 2.2. Spike-triggered averages of recordings from one filiform sensory afferent axon. The top trace is averaged from approximately 1000 recordings from a distal tungsten electrode at the base of a hair. The bottom trace is an average of the corresponding traces recorded simultaneously from the proximal suction electrode on the cercal nerve near the TAG. Scale bar indicates 2 ms.

Each point on the graph in Figure 3 corresponds to a measurement of the spike propagation latency between the distal recording site and the base of the cercus for a single afferent axon, plotted against the distance between these two sites. The dashed line is the best-fit linear regression through the data pooled across all samples. The slope of the regression line corresponds to an axonal spike propagation speed of 1.87 +/- 0.09 mm/ms ($R^2 = 0.96$, $p < 0.001$). There was no significant difference in conduction speeds within this sample of 23 measurements, either within or between animals, between different hair lengths, or between different locations of the sensor out along the cerci. Technical difficulties largely limited us to measuring from

hairs on the dorsal surface. However, the few conduction delay measurements obtained from hairs on other cercal surfaces are in agreement with the above reported conduction velocities. Inverting this velocity value yields a spike conduction time of 0.54 ms/mm of axon. Over the 10 mm length of a typical adult cercus, this spike propagation speed translates to a differential propagation latency of approximately 5 ms between the most proximal and the most distal filiform hairs.

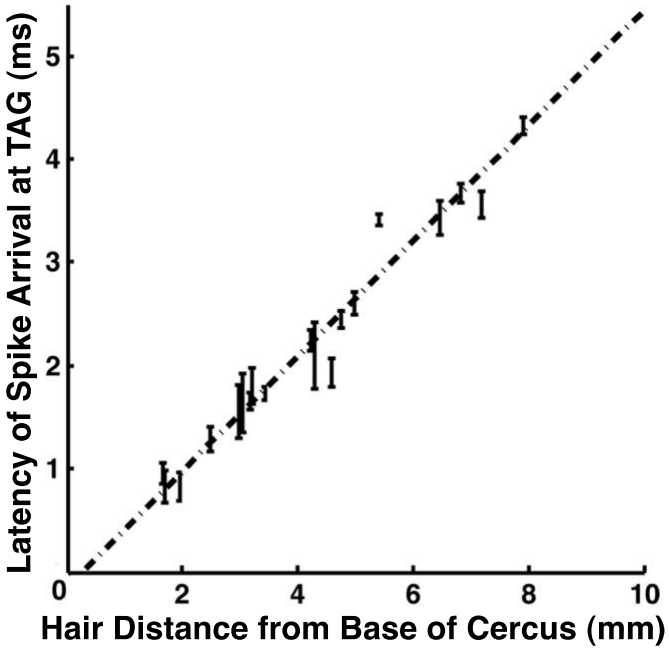

Figure 2.3. Linear dependence of spike propagation time on sensory afferent axon length. Each point on this graph is the spike propagation latency between the distal recording site and the base of the cercus for a single afferent axon, plotted against the distance between these two sites. Error bars show the standard deviation of latencies measured for each hair. The dashed line is the best-fit linear regression for 23 hairs on 6 animals. The slope of the regression line measures the average axonal conduction velocity: 1.87 +/- .09 mm/ms ($R^2 = 0.96$, $p < 0.001$). This corresponds to a differential conduction delay of 0.54 ms/mm, or 5.4 ms over the length of a typical adult cercus.

Ensemble Response of the Filiform Sensory Afferent Array to Sequenced Stimuli

Most (if not *all*) behaviorally-relevant air current stimuli activate the entire ensemble of approximately 1500 filiform hairs distributed across both of the two cerci of a cricket. Given the observed range of spike conduction latencies, we would expect that the ensemble response of the entire afferent array to any specific stimulus would arrive at the terminal abdominal ganglion as a distribution of spikes, with a width that depends on the specific dynamical characteristics of the stimulus. Due to the differential spike propagation latencies caused by the length of the cerci, we would expect an impulsive step-function-like displacement of the entire block of air surrounding a cercus to elicit a train of afferent spikes that would be dispersed within a minimum of a 5 ms interval upon arrival at the TAG. Air current wavefronts that swept along the length of a cercus would be expected to either increase or decrease the dispersion of the spike distribution. In particular, a wave front traveling from the tip of a cercus toward the base of the cercus at a speed near 2 mm/ms would be expected to compress the spike distribution, whereas a wave front traveling at that same speed but in the opposite direction (*i.e.*, from cercus base to tip) would disperse the distribution.

To test these hypotheses, we measured the ensemble spike train responses of cercal sensory afferents in a cercal nerve during the presentation of a variety of air current stimuli that mimicked these different scenarios, *i.e.*, bulk air movement across the entire cercus, and wavefronts moving at different directions and speeds along the cercus. This was accomplished through the presentation of sets of four independent air current jets, directed at equally-spaced positions along the cercus, either simultaneously (to mimic bulk flow) or in timed sequences (to mimic traveling wavefronts), as described in the Methods section. These jets were positioned as

in Figure 1 to activate primarily axial moving hairs on the medial and lateral cercal surfaces. This further allowed us to test whether the consistent conduction delays observed above for hairs on the dorsal cercal surface could be generalized to all filiform cercal hairs.

Figure 4 shows three examples of the ensemble afferent responses to different stimulus sets. In each panel, the upper trace shows the timing of the four independent air current jets, all of which were half-cosine waveforms of the same amplitude and duration. The lower trace in each panel shows the average of 200 cercal nerve responses to repeated presentations of the corresponding stimulus sequence. The central panel (B) serves as the control case and shows the cercal nerve response to a stimulus in which all four positions along the cercus were activated simultaneously (resulting in a superposition of the four half-cosine waveforms into a single peak). This set was equivalent to a uniform bulk air displacement, similar to those that have been used in all previous studies that used standard loudspeakers to generate bulk airflow over an entire cricket specimen. The averaged compound spike waveform is distributed over an interval of approximately 10 ms.

Panel A shows the average compound waveform response to a stimulus sequence that started at the base of a cercus and swept toward the tip of the cercus, *i.e.* opposite to the direction of spike propagation along the cercus. The base stimuli preceded the tip stimuli by 5ms. As expected, the spikes were dispersed to an even greater extent than observed for the control (simultaneous) case shown in panel B, over an interval of approximately 15-18 ms.

Panel C shows the average compound waveform response to a stimulus sequence that started at the tip of a cercus and swept toward the base of the cercus. The tip-to-base delay time was 5 ms, equivalent in duration to the 5 ms differential spike conduction delay time calculated

from the previous set of experiments. This stimulus sequence yielded an ensemble response which was clearly greater in amplitude and shorter in duration than those in the other panels. The spikes originating from hairs at all different locations along the cercus appeared to fuse into a compound waveform resembling a single action potential at the recording site at the base of the cercal nerve.

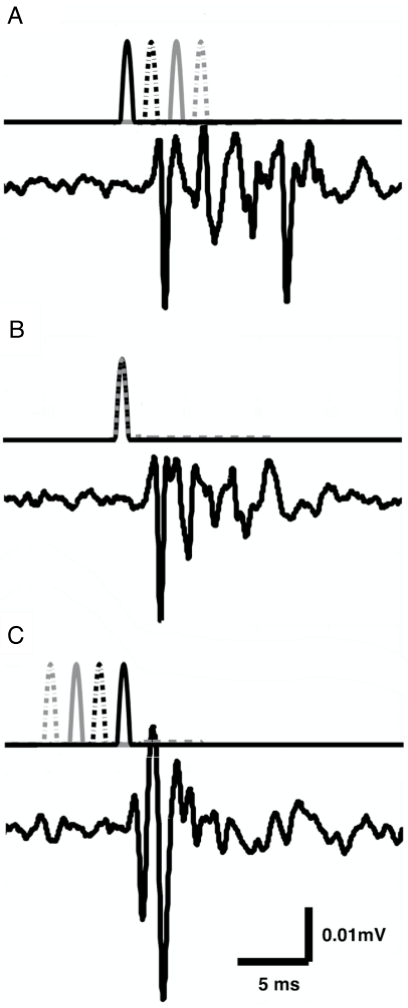

Figure 2.4. Dispersion of the ensemble response of the filiform sensory afferent array. In each panel, the upper trace plots the stimulus waveforms driving four independent air jets through four nozzles aligned along a cercus. Each jet was a unidirectional half-cosine waveform of duration 1.25 ms, adjusted in amplitude to be just supra-threshold for elicitation of spikes as observed on the extracellular electrode at the base of the cercal nerve. The waveform for each nozzle is shown

with a different line type: the solid black line is for the first nozzle at the base of the cercus, the dashed black line is for the second nozzle 3.3 mm out from the base, the solid gray line is for the third nozzle 6.7 mm out from the base, and the dashed gray line is for the fourth nozzle at the distal tip of the cercus. Note that in panels A and C, the puffs were separated in time and were therefore separable on the top traces. In panel B the puffs were presented simultaneously and were therefore superimposed. The lower trace in each panel shows the average of 200 cercal nerve responses to repeated presentations of the corresponding stimulus sequence. A. Average ensemble response of the cercal nerve to a stimulus sequence that started at the base of a cercus and swept toward the tip of the cercus, *i.e.*, opposite to the direction of spike propagation along the cercus, with base-to-tip delay of 5 ms. B. Average ensemble response of the cercal nerve to a stimulus in which all four positions along the cercus were activated simultaneously. C. Average ensemble response of the cercal nerve to a stimulus sequence that started at the tip of a cercus and swept toward the base of the cercus, *i.e.*, in the direction of spike propagation along the cercus, with tip-to-base delay of 5 ms.

Measurements were repeated for a variety of sequence intervals ranging between 0 and 10 ms in half-ms increments, and in both directions along the cerci, for five crickets. In all cases, the stimulus sequence with 5 ms total delay from tip to base elicited the average compound response having the largest peak amplitude. We interpret this as corresponding to the highest degree of synchronous arrival of the elicited spikes at the recording site.

Responses of Primary Cercal Sensory Interneurons to Sequenced Stimuli

The primary synaptic targets of the cercal filiform afferents are a set of sensory interneurons in the terminal abdominal ganglion. All of the information that is extracted by this system and conveyed to higher CNS levels is carried through the axons of approximately twenty of these INs, which project through the paired abdominal connectives to ganglia in the thorax and head. All of our previous studies of these INs have been based on experiments using bulk flow air current stimuli, *i.e.*, stimuli that simultaneously activate all filiform hairs along the entire length of the cerci. Here we tested whether any of the projecting INs had differential sensitivity to the differently-timed sequences of air puffs used for the experiments described in the

preceding section. To do so, the stimulus sequences were presented while we recorded the spiking activity through one abdominal hemi-cord in each of eight animals. We were able to obtain unequivocal discrimination of up to thirteen different units in these preparations, using simultaneous extracellular recordings from five points along the abdominal nerve cord as the basis for phased-array spike sorting (see Methods). Air current stimuli elicited reliable spiking responses in ten of these thirteen units.

Of these ten air-current-sensitive INs, seven showed some degree of differential sensitivity to the direction and speed of the simulated wave front. Figure 5 shows examples of stimulus-evoked responses of three different cercal interneurons, which are representative of three broad classes of IN responsiveness we observed. Each of the three colors in the panels is associated with data from a different one of the three cells, and each vertical panel is associated with a different stimulus sequence. The upper trace in each panel shows the timing of the four independent air current jets, all of which were half-cosine waveforms of the same amplitude and duration as in the experiments associated with Figure 4. Below each stimulus trace are raw data traces recorded from three of the five extracellular electrodes placed along the abdominal nerve cord during presentation of that stimulus sequence. Spikes were recorded for 50 repeated presentations of each stimulus sequence and discriminated on the basis of their waveforms and propagation velocities to obtain a series of spike times for each individual cell. A raster plot showing the stimulus-elicited spike occurrence times for three different INs for 50 stimulus presentations is shown below the raw data traces. Histograms for the occurrence times of spikes elicited from these three different cells are shown at the bottom of each vertical panel.

Each of these cercal INs had a different characteristic responsiveness to the three different stimulus sequences. The simplest case was that of the cell represented with the red markers and red histograms. This cell was equally responsive to all three stimulus sequences, in terms of the number of spikes elicited per stimulus and the distribution of those spikes in time following the stimulus. The other two cells (represented by black and blue markers and histograms) showed substantial sensitivity to the timing of the air current puff sequences. Both of these units were activated reliably by the set of pulses sweeping from the tip of the cercus to the base at a speed equivalent to the average propagation speed of the filiform afferent axons (panel C). Note, however, that the temporal distributions of elicited spikes were quite different in these two cells. For simultaneous puffs mimicking bulk-flow stimuli (panel B), the responses of the cells were quite different from one another: although the activity of the cell indicated with red markers changed very little from the case in panel C, the reliability of the unit represented with black markers dropped to below 0.5, and the unit corresponding to the blue data points was essentially unresponsive. For the set of four pulses sweeping from the base of the cercus to the tip (panel A), the cell indicated with black markers was even less responsive, but the cell indicated with blue markers showed significant responsiveness.

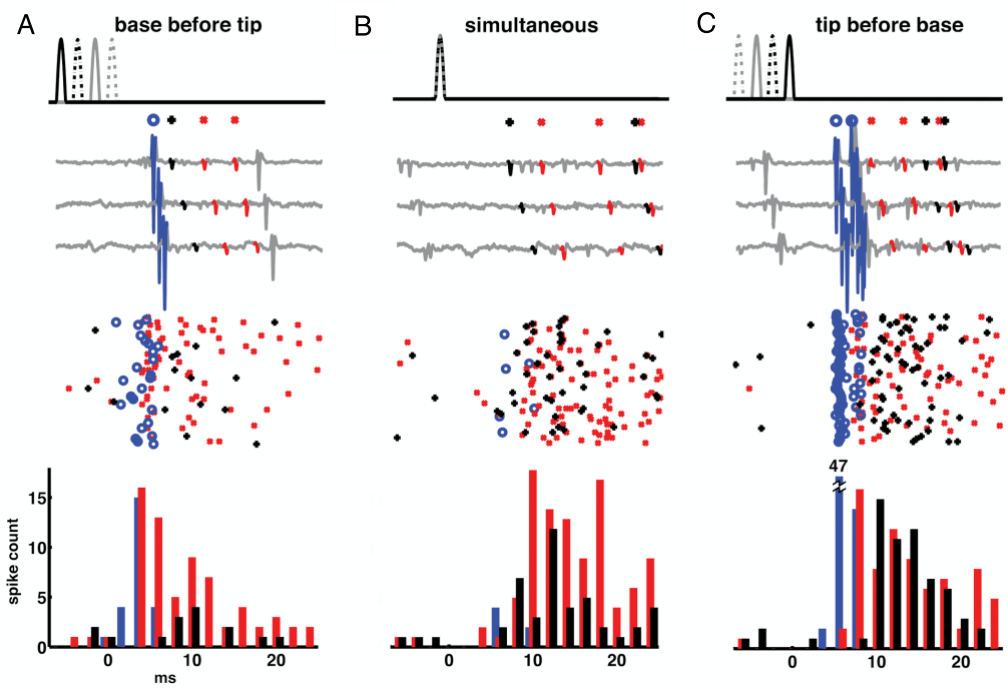

Figure 2.5. Response of projecting interneurons to stimulus jet sequences along the cercus. In each of the three panels, the upper trace plots the stimulus waveforms driving four independent air jets through four independent nozzles aligned along a cercus. Each jet was a unidirectional half-cosine waveform of duration 1.25 ms, adjusted to the same amplitude as used for Figure 4. The waveform for each nozzle is shown with a different line type. As in Figure 4, the solid black line is for the first nozzle at the base of the cercus, the dashed black line is for the second nozzle 3.3mm out from the base, the solid gray line is for the third nozzle 6.7 mm out from the base, and the dashed gray line is for the fourth nozzle at the distal tip of the cercus. Below each stimulus trace are raw electrophysiological recordings from three of the five extracellular electrodes placed along the abdominal nerve cord during presentation of that stimulus sequence. The top traces are from the electrode closest to the TAG, and the bottom traces are from the electrode farthest from the TAG. Segments of these traces are color-coded for three of the fourteen different units that were discriminated. Below each set of recordings is a raster plot showing the stimulus-elicited spike occurrence times for the three different color-coded INs elicited by fifty repeated stimulus presentations. The bottom plot for each panel is a histogram (with 2ms time bins) for the occurrence times of spikes elicited from these three different cells. A. IN responses to stimulus sequences that started at the base of a cercus and swept toward the tip of the cercus, *i.e.*, opposite to the direction of spike propagation along the cercus, with base-to-tip delay of 5ms. B. IN responses to stimuli in which all four positions along the cercus were activated simultaneously. C. IN responses to stimulus sequences that started at the tip of a cercus and swept toward the base of the cercus, *i.e.*, in the direction of spike propagation along the cercus, with tip-to-base delay of 5 ms.

A more comprehensive representation of the dynamic sensitivities of these three cercal interneurons is shown in Figure 6. These graphs plot the relative responsiveness of the three INs to multi-air-jet stimulus sequences that were swept along the cercus over a wide range of velocities. Each of the three colored plots in this figure is color-matched to one of the cells in Figure 5. A single data point on a plot indicates that cell's mean response to fifty repeated presentations of a specific 4-jet sequence. For instance, the data point marked with an asterisk near the left end of the red plot in Figure 6 was calculated from the data set corresponding to the red-colored unit in panel A of Figure 5. Responses were calculated by counting the mean number of spikes occurring within a 25 ms window after the presentation of the last of the four stimulus jets in that particular sequence set, and then normalizing that value to the mean spike count recorded for the stimulus sequence that yielded the maximal response. Error bars indicate one standard deviation around the mean. Two different scales are presented for the abscissa. The black ordinate scale corresponds to the time between the first and last stimulus puff, with positive numbers indicating that the cercal tip was stimulated first (*i.e.*, 0 corresponds to simultaneous presentation of the four pulses, positive values correspond to tip-to-base sweeps, and negative values correspond to base-to-tip sweeps; a total delay of +5ms corresponds to the conduction velocity of the filiform afferents.) The green scale translates these delays into simulated wavefront velocities. (The velocity is simply the 1cm length of the cercus divided by the total delay time between the tip and base pulses.) Note that we sampled the range between 1ms tip lead and 1ms base lead at a finer resolution and displayed an expanded scale in this range for improved visibility.

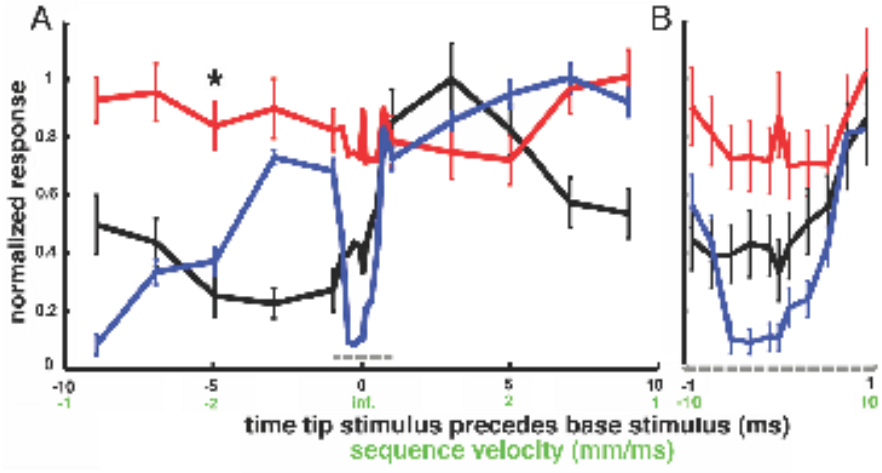

Figure 2.6. Differential behavior of INs to simulated wave fronts. The three plots show the responses of three INs to a set of multi-air-jet stimulus sequences presented at a variety of sweep speeds and directions. The three cells are the same as those described in Figure 4, and the same color-coding is used. The ordinate is the mean number of elicited spikes (counted within 25 ms after stimulus termination) for fifty repeated presentations of the corresponding stimulus sequence, normalized by the spike count recorded for the stimulus sequence that yielded the maximal response. Error bars indicate one standard deviation around the mean. The abscissa indicates the speed with which the stimulus jets were swept along the cercus. Two different scales are presented for the abscissa. The black ordinate scale corresponds to the time between the first and last stimulus jet, with positive numbers indicating that the cercal tip was stimulated first (i.e., 0 corresponds to simultaneous presentation of the four pulses, positive values correspond to tip-to-base sweeps, and negative values correspond to base-to-tip sweeps; a total delay of +5 ms corresponds to the conduction velocity of the filiform afferents.) The green scale translates these delays into simulated wavefront velocities. Note that the range between 1 ms tip lead and 1ms base lead is displayed at an expanded ordinate scale for improved visibility.

The IN represented with the red plot in Figure 6 responds with approximately the same number of spikes to stimulus sequences at all sweep velocities, as well as to bulk flow stimuli. As can be seen in Figure 5, this cell fires at a fixed latency from stimulation at the cercal base. The IN represented with the black plot was activated best by sets of four pulses sweeping from the tip of the cercus to the base at speeds between 1 and 5 mm/ms, which is near the average propagation speed of the filiform afferent axons. Its responsiveness decreases by about 50% as stimulus sequence velocities approach 0 (i.e., the bulk-flow case). Its minimum responsiveness is for stimulus sequences that sweep from base to tip at speeds between 1 and 5 mm/ms.

The IN represented with the blue plot has the most complex differential sensitivity to the directional sequences. This cell was activated strongly and reliably by all sets of four pulses sweeping from the tip of the cercus to the base at speeds above 0.5 mm/ms. Its responsiveness dropped sharply to almost zero for stimulus sequence velocities within +/- 0.5 mm/ms of the bulk-flow case. However, it was also reliably responsive for stimulus sequences that swept from base to tip at speeds of less than 5 mm/ms.

Experiments were replicated using a total of eight cricket specimens. Cells with equivalent dynamic sensitivities to the three shown in Figures 5 and 6 were observed in all preparations. We did not characterize the stimulus-response characteristics of the other seven air-current-sensitive units we discriminated to the same degree of precision as for the three units presented in these figures. However, we note that the stimulus-response sensitivities of all of the ten units we observed could be divided into the following general classes: three cells showed no significant differential responsiveness to different multi-jet stimulus sequences, and the remaining seven cells showed significant selective responsiveness to stimulus sequences advancing from the tip of the cercus toward the base of the cercus. Of these seven cells, two showed substantial selective suppression of responsiveness to simultaneous air jets (*i.e.*, "bulk flow" stimuli).

Discussion

The general goals of our study were to determine the extent to which the distribution of receptor hairs out along the length of the cerci leads to temporal dispersion of the receptors' spike trains upon entry into the TAG, and to investigate the functional significance of the observed dispersion. The results presented here demonstrate that the differential conduction

characteristics of the filiform receptor array are of substantial significance: the cerci operate as delay-lines, and their functional organization supports computations by identified interneurons that have not been realized in earlier studies. These results force a substantial revision of our understanding of the structural and functional organization and operation of this system.

Cricket Cerci Function as Delay-Lines

We report a mean spike propagation speed for the cercal filiform afferent fibers of approximately 1.9 mm/ms. This is consistent with the fastest values reported for other insect sensory axons of equivalent diameter (Chapman and Pankhurst, 1967; Pumphrey and Rawdon-Smith, 1937). While the value of the conduction velocity is likely selected only to be as rapid as allowed given energetic constraints, the observed variance across neurons or across animals is quite small. The extremely low intra- and inter-animal variance around the mean conduction speed ($R^2 = 0.96$ at the 0.001 level), the functional organization of the cercal filiform sensory array could, in theory, support subsequent computations based on the observed delay-line characteristics. The cercal sensory system therefore shares common operational features with several other sensory systems that are implemented around delay-line processing (Beckius et al., 1999; Carr et al., 1986; Carr, 1993; Carr and Konishi, 1988; Saitoh and Suga, 1995; Schnupp and Carr, 2009). Our results suggest that the diameters of the filiform afferents may be extremely uniform, within and between animals. To our knowledge, however, there has been no systematic anatomical analysis of filiform afferent axon diameters. The only published anatomical data concerning afferent axons in *Acheta domesticus* were derived from a single cross-section of a cercal nerve, and the authors were unable to identify the subset of the axons that corresponded to the filiform afferents (Edwards and Palka, 1974).

This delay-line phenomenology is not surprising in and of itself: delay-line characteristics would be expected from a linear sensor array, if the spike propagation velocity were nearly equal in all afferent axons. We note, however, that our results are in direct contrast to those reported recently for a linearly-distributed array of sensory afferent axons in an analogous system in the crayfish (Mellon and Christison-Lagay, 2008). A population of hydrodynamic mechanoreceptors located on the antennules of *Procambarus clarkii* drives the initiation of the animal's startle response. Although the mechanoreceptors are distributed along the crayfish antennules, afferent spikes generated in this sensory array by bulk fluid movements arrive simultaneously at the central integration site. This simultaneity results from position-dependent variations in the sensory-axon conduction velocities, which appears to derive from a systematic graduated increase in axon diameter for more distally located sensilla. It may be that the relative incompressibility of water would lead to most signals arriving simultaneously for the crayfish while they could be distributed in air for the cricket. Similar mechanisms underlying a systematic gradation in conduction velocity that result in neuronal synchrony have also been demonstrated in mollusks (Young, 1939) and vertebrates (Bennett, 1971; Sugihara et al., 1993).

Although the presence of some degree of differential delay-line phenomenology might have been expected in the cercal system, to the best of our knowledge neither its timescale nor its variance had been measured in previous studies, nor had the possible functional implications of delay-line characteristics been considered. It should be expected that a temporal dispersion of 5ms would be of considerable functional significance. To illustrate, consider the response of filiform afferents to stimulus components at 100 Hz: spikes from the distal tip of the cercus would be arriving at the TAG at a phase delay of one-half cycle with respect to the spikes from

the proximal end, and an un-compensated summation of the spikes from the full extent of the cercus would result in a partial temporal demodulation of the signals. If no computational mechanisms functioned to compensate for this dispersion, then the effective range over which the cercal system could demonstrate differential frequency sensitivity would be limited to signals below approximately 100 Hz. This is certainly not the case: the behaviorally-relevant differential frequency range for the cricket cercal system is known to extend to at least 600 Hz (Tauber and Camhi, 1995). This implies that some form of functional compensation must be implemented in at least some of the sensory interneurons.

Some Interneurons Are Sensitive to the Direction and Speed of Stimulus Wave Fronts

We obtained clear discrimination of ten units that were sensitive to air currents in our preparations. This number of ten units corresponds to the expected number of cercal projecting interneurons that run through each hemi-connective. Although our use of extracellular recording techniques did not allow unequivocal identification of the air-current-sensitive units with respect to the ten known classes of re-identifiable interneurons, we conclude that the units we describe in detail in Figures 5 and 6 are among the identified cercal INs that have been described in previous studies (Jacobs and Murphey, 1987).

As indicated above, the stimulus-response characteristics of three cells described in Figures 5 and 6 are representative of the three different general classes of responsiveness observed in our experiments. It is also worth noting that the relative firing rates of the three cells in Figure 6 provide sufficient information to discriminate stimuli moving proximally from those moving distally or occurring simultaneously. The class with the least complex responsiveness is exemplified by the cell represented with the red symbols and plots in Figures 5 and 6. That cell

had no significant differential sensitivity to any of the different stimulus sequences: it always fired in phase with the one jet delivered to the base of the cercus. We hypothesize that this IN makes differential synaptic connectivity with the subset of filiform afferents innervating the dense group of mechanosensory hairs at the base of the cercus.

The responsiveness of the cell represented with the black symbols and lines in Figures 5 and 6 is also easily understandable within the context of the observed afferent delay-line characteristics. The amplitude of this cell's response was greatest for stimulus sequences that swept along the cercus from tip to base at a speed near the spike propagation speed. The responsiveness decreased to less than half of the best response for simultaneous (bulk-flow) stimuli and decreased even further for stimuli that swept along the cercus in the base-to-tip direction (i.e., opposite to the spike propagation direction). No special dendritic structure or synaptic connectivity would be required for this cell to function as a "filter" for such sweeps: a simple linear summation of all inputs, processed with a threshold, would yield this characteristic sensitivity. That is, the delay-line characteristics of the cercal afferent array could be sufficient for the observed dynamic sensitivity of this IN. In the engineering sense, this cell appears to function as a "phased array detector."

The characteristic sensitivity for the cell represented with the blue symbols and plots in Figures 5 and 6 is more complex from a mechanistic standpoint. This cell was approximately equally responsive to all stimulus sequences that swept along the cercus from tip to base, regardless of sequence speed. However, the responsiveness dropped effectively to zero for a small range of stimulus sequence speeds bracketing the bulk-flow case, and then returned to as much as 80% of the best response for a range of stimulus sequences that swept from base to tip.

In the engineering sense, this cell appears to function as a “notch filter,” in a manner that would filter out the responses of the receptor array to bulk flow of the air around the animal. The behavioral significance of this filtering operation could be very straightforward: the animal’s own movements would generate such bulk air movements, as would any large-scale air movements caused by wind or movements of near-by large objects. This cell is therefore a candidate for involvement in subsequent computations requiring small-scale dynamic feature detection.

Some aspect of this neuron’s dendritic structure and/or synaptic integrative properties results in its being “tuned” to (or to filter out) a particular dynamic activation sequence along the cerci *other* than the one sequence that yields the largest linear sum through delay-line-based superposition. Several plausible biological mechanisms can be imagined through which this cercal IN (and similar INs) could achieve such complex dynamical sensitivity. These mechanisms would require that the interneuron has dendritic architecture that would enable segregation of the synaptic inputs from the different afferents on the basis of their cercal location. This segregation could be used to enhance discrimination of dynamic aspects of stimulus waveforms that are smaller than the spatial scale of a single cercus. For example, configurations can be imagined that would use the delay-line characteristics of the cercus to directly discriminate the direction of air current wavefronts traveling toward or away from the animal at speeds in the range 1cm/5ms, in a manner equivalent to that proposed by Rall (Rall, 1964). This would require the synaptic arbors of afferents from distal hairs to project into regions of the filiform map that are distinct from the arbors of similar hairs located at proximal locations on the cercus. Such a location-based topographic segregation of afferent arborizations has not

been considered in earlier anatomical characterizations of the afferent map (Bacon and Murphey, 1984; Jacobs and Theunissen, 1996). Multi-cellular-circuit-based mechanisms might also be involved in producing the complex dynamical sensitivities observed in this cell.

Considering the possible functional implications of differential latency of afferents from different locations out along the cerci, it will be important to determine if the filiform sensory afferents are in fact segregated and/or labeled in a manner that would allow such differential connectivity to the INs. The electrophysiological response properties and anatomy of the filiform sensory afferent arborizations of a sample of the filiform receptors have been studied previously (Jacobs and Theunissen, 1996; Paydar et al., 1999), and used as the basis for predicting the global activity patterns which would be elicited across the ensemble of afferent terminals in response to several types of air current stimuli (Jacobs and Pittendrigh, 2002; Jacobs and Theunissen, 2000). The mechanoreceptors used for those previous studies were all located near the base of the cerci. Subsequent modeling studies made the implicit assumption that cercal interneurons integrate sensory input from filiform afferents with no consideration of any systematic temporal dispersion (Jacobs and Pittendrigh, 2002; Jacobs and Theunissen, 2000; Magal et al., 2006). Based on the results presented here, it will be necessary to refine the anatomical atlas to incorporate the information regarding cercal delay-line properties. This will, in turn, enable a more accurate representation of the dynamic activity patterns for modeling studies of the primary interneurons that are the decoders of the afferent input.

Acknowledgements

This work was supported by NIH/NSF grant CRCNS-0515290, NSF Grant CMMI-0849433, and NSF Grant EF-0425878. We thank Tomas Gedeon and Gwen Jacobs for helpful discussions and comments.

References

Bacon, J.P., Murphey, R.K., 1984. Receptive fields of cricket giant interneurones are related to their dendritic structure. The Journal of Physiology 352, 601–623. https://doi.org/10.1113/jphysiol.1984.sp015312

Beckius, G.E., Batra, R., Oliver, D.L., 1999. Axons from anteroventral cochlear nucleus that terminate in medial superior olive of cat: Observations related to delay lines. J. Neurosci. 19, 3146–3161. https://doi.org/10.1523/JNEUROSCI.19-08-03146.1999

Bennett, M., 1971. Electric organs, in: Fish Physiology. Academic Press, New York, pp. 347–491.

Carr, C., Heiligenberg, W., Rose, G., 1986. A time-comparison circuit in the electric fish midbrain. I. Behavior and physiology. J. Neurosci. 6, 107–119. https://doi.org/10.1523/JNEUROSCI.06-01-00107.1986

Carr, C.E., 1993. Processing of temporal information in the brain. Annu. Rev. Neurosci. 16, 223–243. https://doi.org/10.1146/annurev.ne.16.030193.001255

Carr, C.E., Konishi, M., 1988. Axonal delay lines for time measurement in the owl's brainstem. Proceedings of the National Academy of Sciences 85, 8311–8315. https://doi.org/10.1073/pnas.85.21.8311

Casas, J., Steinmann, T., Dangles, O., 2008. The aerodynamic signature of running spiders. PLoS ONE 3, e2116. https://doi.org/10.1371/journal.pone.0002116

Chapman, K.M., Pankhurst, J.H., 1967. Conduction velocities and their temperature coefficients in sensory verve fibres of cockroach jegs. Journal of Experimental Biology 46, 63–84. https://doi.org/10.1242/jeb.46.1.63

Comer, C., Mara, E., Murphey, K., Getman, M., Mungy, M., 1994. Multisensory control of escape in the cockroach Periplaneta americana. Journal of Comparative Physiology A 174, 13–26.

Dangles, O., Irschick, D., Chittka, L., Casas, J., 2009. Variability in sensory ecology: expanding the bridge between physiology and evolutionary biology. The Quarterly Review of Biology 84, 51–74. https://doi.org/10.1086/596463

Dangles, O., Ory, N., Steinmann, T., Christides, J.-P., Casas, J., 2006. Spider's attack versus cricket's escape: velocity modes determine success. Animal Behaviour 72, 603–610. https://doi.org/10.1016/j.anbehav.2005.11.018

Edwards, J., Palka, J., 1974. The cerci and abdominal giant fibres of the house cricket, *Acheta domesticus* . I. Anatomy and physiology of normal adults. Proc. R. Soc. Lond. B. 185, 83–103. https://doi.org/10.1098/rspb.1974.0007

Gnatzy, W., Heusslein, R., 1986. Digger wasp against crickets: I. Receptors involved in the antipredator strategies of the prey. Naturwissenschaften 73, 212–215. https://doi.org/10.1007/BF00417728

Gnatzy, W., Kamper, G., 1990. Digger wasp against crickets. II. An airborne signal produced by a running predator. J Comp Physiol A 167. https://doi.org/10.1007/BF00190826

Heinzel, H.-G., Dambach, M., 1987. Travelling air vortex rings as potential communication signals in a cricket. J. Comp. Physiol. 160, 79–88. https://doi.org/10.1007/BF00613443

Huang, Y., Miller, J., 2004. Phased-array processing for spike discrimination. Journal of Neurophysiology 92, 1944–1957.

Jacobs, G., Pittendrigh, C., 2002. Predicting emergent properties of neuronal ensembles a database of individual neurons, in: Computational Neuroanatomy. Humana Press, Totowa, NJ, pp. 151–170.

Jacobs, G., Theunissen, F., 1996. Functional organization of a neural map in the cricket cercal sensory system. J. Neurosci. 16, 769–784. https://doi.org/10.1523/JNEUROSCI.16-02-00769.1996

Jacobs, G.A., Miller, J.P., Aldworth, Z., 2008. Computational mechanisms of mechanosensory processing in the cricket. Journal of Experimental Biology 211, 1819–1828. https://doi.org/10.1242/jeb.016402

Jacobs, G.A., Murphey, R.K., 1987. Segmental origins of the cricket giant interneuron system. J. Comp. Neurol. 265, 145–157. https://doi.org/10.1002/cne.902650110

Jacobs, G.A., Theunissen, F.E., 2000. Extraction of sensory parameters from a neural map by primary sensory interneurons. J. Neurosci. 20, 2934–2943. https://doi.org/10.1523/JNEUROSCI.20-08-02934.2000

Kamper, G., Dambach, M., 1981. Response of the cercus-to-giant interneuron system in crickets to species-specific song. J. Comp. Physiol. 141, 311–317. https://doi.org/10.1007/BF00609933

Landolfa, M., Jacobs, G., 1995. Direction sensitivity of the filiform hair population of the cricket cercal system. Journal of Comparative Physiology A 177, 759–766.

Magal, C., Dangles, O., Caparroy, P., Casas, J., 2006. Hair canopy of cricket sensory system tuned to predator signals. Journal of Theoretical Biology 241, 459–466. https://doi.org/10.1016/j.jtbi.2005.12.009

Mellon, D., Christison-Lagay, K., 2008. A mechanism for neuronal coincidence revealed in the crayfish antennule. Proceedings of the National Academy of Sciences 105, 14626–14631. https://doi.org/10.1073/pnas.0804385105

O'Shea, M., Adams, M.E., 1981. Pentapeptide (proctolin) associated with an identified neuron. Science 213, 567–569. https://doi.org/10.1126/science.6113690

Palka, J., Levine, R., Schubiger, M., 1977. The cercus-to-giant interneuron system of cricket. Journal of Comparative Physiology A 119, 267–283.

Paydar, S., Doan, C.A., Jacobs, G.A., 1999. Neural mapping of direction and frequency in the cricket cercal sensory system. J. Neurosci. 19, 1771–1781. https://doi.org/10.1523/JNEUROSCI.19-05-01771.1999

Pumphrey, R., Rawdon-Smith, A., 1937. Synaptic transmission of nervous impulses through the last abdominal ganglion of the cockroach. Proc. R. Soc. Lond. B 122, 106–118. https://doi.org/10.1098/rspb.1937.0013

Rall, W., 1964. Theoretical significance of dendritic trees of neuronal input-output relations, in: Neural Theory and Modeling. Stanford University Press, Palo Alto, CA, pp. 73–97.

Saitoh, I., Suga, N., 1995. Long delay lines for ranging are created by inhibition in the inferior colliculus of the mustached bat. Journal of Neurophysiology 74, 1–11. https://doi.org/10.1152/jn.1995.74.1.1

Schnupp, J.W.H., Carr, C.E., 2009. On hearing with more than one ear: lessons from evolution. Nat Neurosci 12, 692–697. https://doi.org/10.1038/nn.2325

Shimozawa, T., Kanou, T., 1984. The aerodynamics and sensory physiology of range fractionation in the cereal filiform sensilla of the cricket Gryllus bimaculatus. Journal of Comparative Physiology A 155, 495–505.

Sugihara, I., Lang, E.J., Llinás, R., 1993. Uniform olivocerebellar conduction time underlies Purkinje cell complex spike synchronicity in the rat cerebellum. The Journal of Physiology 470, 243–271. https://doi.org/10.1113/jphysiol.1993.sp019857

Tauber, E., Camhi, J., 1995. The wind-evoked escape behavior of the cricket Gryllus bimaculatus: integration of behavioral elements. J Exp Biol 198, 1895–1907.

Young, J., 1939. Fused neurons and synaptic contacts in the giant nerve fibres of cephalopods. Phil. Trans. R. Soc. Lond. B 229, 465–503. https://doi.org/10.1098/rstb.1939.0003

CHAPTER THREE

ENCODING OF SMALL-SCALE AIR MOTION DYNAMICS IN THE CRICKET *ACHETA DOMESTICUS*

Contribution of Authors and Co-Authors

Manuscript in Chapter 3

Author: Jonas L. Mulder-Rosi

Contributions: Designed the study, carried out the experiments, analyzed the data, and wrote the manuscript

Co-Author: John P. Miller

Contributions: Obtained funding, designed study, discussed ideas, wrote the manuscript

Manuscript Information

Jonas L. Mulder-Rosi, John P. Miller

Status of Manuscript:
_x__ Prepared for submission to a peer-reviewed journal
____ Officially submitted to a peer-reviewed journal
____ Accepted by a peer-reviewed journal
____ Published in a peer-reviewed journal

CHAPTER THREE

ENCODING OF SMALL-SCALE AIR MOTION DYNAMICS IN THE CRICKET *ACHETA DOMESTICUS*

Introduction

The cercal sensory system of the cricket mediates the detection, localization and identification of air-current signals generated by predators, mates and competitors (reviewed in (Jacobs et al., 2008)). This system has been the subject of many anatomical, developmental, functional and theoretical studies over the last four decades. In particular, one set of cercal INs that receive input from the filiform mechanosensory array (INs Left 10-2, Right 10-2, Left 10-3 and Right 10-3) has been the focus of a great many studies based on bulk-flow stimulus-response experimental paradigms (Jacobs and Murphey, 1987). It is thought that this subsystem operates by projecting a coarse-coded image of the stimulus to the ganglia, where feature detection is carried out by more complex, specialized circuits (Butts and Goldman, 2006; Miller et al., 1991; Salinas and Abbott, 1994; Theunissen et al., 1996; Theunissen and Miller, 1991).

In this study, we examined the response characteristics of INs Left 10-2, Right 10-2, Left 10-3 and Right 10-3 to a much broader, more complex, and more behaviorally relevant stimulus space than has been used in the past and have come to very different conclusions about several fundamental aspects of the functional roles and operation of these cells. Using a novel stimulating apparatus, we produced temporally complex multi-directional air movements having spatial resolution finer than the scale of the cercal array. We demonstrate that these four INs respond with high sensitivity to complex dynamic multi-directional, small-scale features of air

currents. The velocity threshold for these features is substantially lower than the threshold for simple unidirectional bulk flow stimuli used in previous studies. Thus, some significant small-scale dynamic feature detection is being carried out at the level of the primary sensory interneurons.

Materials and Methods

Animals

Female *Acheta domesticus* crickets from Bassets Cricket Ranch (Visalia, CA) or Timberline Fisheries (Marion, IL) were co-housed and subject to a 12-12 light/dark schedule. Within 10 hours of their final molt crickets were isolated and prepared for recording. Wings, legs, head, and a section of the dorsal thorax and abdomen were removed. Internal viscera were also removed to expose the ventral nerve cord. The nerve cord was then freed from the body and a ventral incision made along the entire length of the thorax and abdomen. The reduced preparation was placed on a holder consisting of eight fine insulated wires (California Fine Wire) stretched over a 3-mm gap between polyethylene sidewalls. Each wire had a small segment from which the insulation had been removed. The ventral nerve cord was placed over these exposed areas and electrically isolated using a 7:3 mixture of Vaseline and mineral oil. The left connective was cut anterior to the terminal abdominal ganglion to limit the number of unique units that had to be differentiated. In a few cases, the right connective was cut, and angular and left-right time delay data were flipped. This allowed us to check for lateral differences in the left and right hemi ganglia. The abdominal cavity was filled with saline and the preparation arranged so that the cercal array extended from the rear of the holder as shown in Figure 1A.

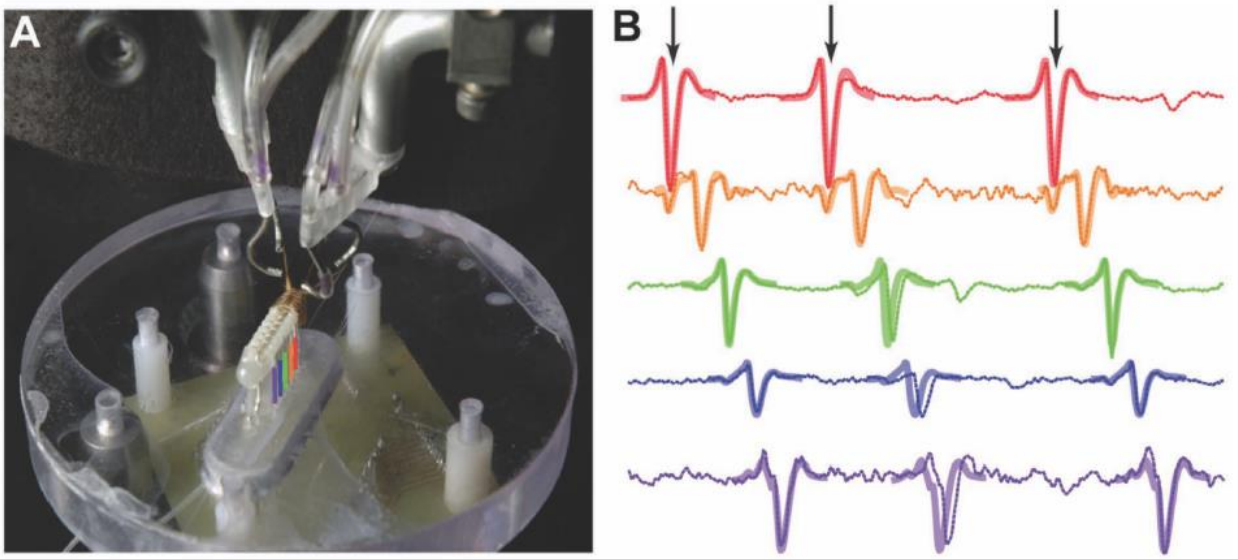

Figure 3.1. Experimental apparatus and spike sorting. (A) The stimulus delivery and electrophysiological recording apparatus. Air current pulses were delivered through a set of four stainless steel nozzles positioned above the cerci. Each nozzle could be rotated independently of the others and delivered short-duration jets of air driven by small computer-controlled speaker cones. Recordings were made from the ventral nerve cord using up to eight extracellular wire electrodes. (B) The fine colored traces are a set of five simultaneous extracellular recordings, color-coded by the distance of their electrodes from the TAG (indicated as colored lines on the electrode array in panel A. Spikes identified through thresholding (black arrows) were compared to templates with a characteristic conduction velocity (thick colored lines superimposed on the recording traces). The second (slower) spike in panel B illustrates the efficacy of using spike conduction velocity in discriminating similar waveforms: this second spike was generated by a different unit than that used to generate the template and was classified independently.

Stimulation

We created a novel stimulus apparatus consisting of four nozzles made from bent and blunted 18-gauge syringe needles (BD, Franklin Lakes, NJ). Each nozzle was connected through plastic tubing to one of four independent headphone speakers (Radio Shack part 273-092, Fort Worth, TX), enabling each nozzle to be driven with an independent stimulus. Each nozzle could be pivoted arbitrarily in the horizontal plane, enabling the presentation of stimuli at four different positions along the cerci, each of which could be generated from a different direction. A typical configuration for the nozzles during an actual experiment is shown in Figure 1A. The stimulus

nozzles were calibrated using a high-sensitivity, low-velocity solid-state anemometer (Microflown Technologies model MFSC-2, Arnhem, The Netherlands).

The air velocity was measured to drop off sharply as a function of distance from the nozzle. Differences in stimulus amplitude produced at the four channels was small (<10%) and corrected for by scaling the input voltages. The air velocity produced at the nozzles was seen to be a linear function of speaker velocity below 550 Hz. For this reason, each stimulus in our experiments was created with a voltage pulse equivalent to a half sinusoid at 525 Hz, which created a unidirectional "puff" through the corresponding nozzle. For each experiment, care was taken to position the apparatus such the nozzles were positioned precisely 1.5 mm above the cerci, as measured with a calibrated micromanipulator. Air puff amplitudes were set to the minimum values that would noticeably increase the probability of spiking in 10-2 and 10-3 at their preferred directions for bulk airflow. This stimulus intensity corresponded to a velocity of 8.3 +/- 1.2 mm/s at the putative edge of the cercal boundary layer for low-velocity stimuli (Cummins et al., 2007).

Two nozzles were positioned above each cercus. One nozzle in each pair was positioned near the tip of the cercus, and the other nozzle of the pair was positioned over the base of the cercus. The same relative positions along the cerci were used in all preparations. The final orientation of each nozzle was measured from static overhead photographs and measured values were used in subsequent analyses. At each angular configuration of the nozzles, sets of four stimulus puffs were presented through the four nozzles, with inter-stimulus delays of either zero or 5 ms. Each angle/delay combination was presented 25 times with delays randomly interleaved and a delay of 500 ms between trials. Between 12 and 68 angle sets were tested per animal. The sequence of

stimulus angle/delay parameters within each experiment was chosen randomly to avoid systematic biases due to adaptation.

Data Collection and Analysis

Extracellular recordings were analyzed using the phased-array spike sorting method published previously (Huang and Miller, 2004), using software developed within our lab. Briefly, extracellular recordings from eight points along the ventral nerve cord provided information about the extracellular spike waveform of several projecting INs. Spike-conduction velocity of each IN unit was determined from the time delays of spike arrival at the different electrodes and used to sort these spikes into individual units (Figure 1B). Spike identification templates included information about extracellular waveform and conduction velocity.

Spikes were identified via an operation based on a threshold of four times the channel noise standard deviation, and each spike was assigned to one of the templates or a "null template" based on the highest correlation match across all channels. If template subtraction failed to reduce the overall signal power in the template window, or if the spike matched the null template, it was discarded. These units were then matched to identified INs in the TAG based on spike amplitude and tuning to bulk airflow. While some smaller units could not be definitively identified, units 10-3 and 10-2 could be reliably identified in all experiments presented here. Other units which showed similar tuning across experiments were considered identifiable across animals, but were not assigned specific identities, and were not used for experiments reported here.

For each experiment, the baseline firing of all INs was determined based on their average firing rate in the 100 ms before stimulus presentations. All experiments where the firing rate of either

L10-2 or L10-3 dropped below 2 Hz (normal baseline 20-30 Hz) were removed on the assumption that the cell was no longer behaving as it would in an intact animal. The response of each cell was measured as the increase in spike rate over the 15 ms after the complete stimulus had been presented. All rates were normalized to the maximum firing rate observed for a given cell in each animal. The experimental repeatability, or intra-animal variance, dominated inter-animal and left-right variance, so results were pooled across animals. Excitatory stimuli were classified as those that resulted in a measured spike rate significantly above baseline based on a chi-squared test using the Benjamini-Hochburg correction.

For all figures, baseline is calculated as the mean firing rate of each animal: a given point on the graph is the mean firing rate across 15 trials minus the mean firing rate for that IN observed throughout the recording. Our criterion for significance is a p-value less than 0.05, assuming the baseline firing is a Poisson process with the observed mean and standard deviation measured for a given experiment.

Anatomical Reconstructions

Jacobs and colleagues have developed quantitative neuroanatomical tools that were used in the current study to estimate and visualize the mapping of cercal sensory receptor afferents onto the dendrites of cercal interneurons. These tools are based on an extensive set of detailed anatomical reconstructions of the sensory afferent synaptic arborizations (Jacobs and Theunissen, 1996; Paydar et al., 1999; Troyer et al., 1994) and cercal interneurons, including 10-2 and 10-3 (Cummins et al., 2003; Jacobs and Pittendrigh, 2002; Jacobs and Theunissen, 2000). All algorithms and computational approaches have been described in detail in these earlier publications.

Results

Differential Spatial Sensitivity Along the Cerci

Our first goal was to determine if different regions of a single cercus display different directional sensitivity characteristics, as suggested by earlier anatomical studies on this sensory system (Bacon and Murphey, 1984; Jacobs and Miller, 1983; Miller et al., 2011). Such differential spatial sensitivity characteristics would support differential sensitivity to complex multi-directional stimuli that have a structural scale smaller than the dimensions of the cerci. Our measurements were achieved by using a custom stimulus apparatus (Figure 1A) to deliver air current pulses independently to different areas along the cercal array. Two independently activated stimulating nozzles were positioned over each cercus, one in a proximal location near the base of the cercus and another at a distal location 8 mm (80% of the total cercus length) out along the cercus toward its tip. Each of nozzle could be oriented to deliver air pulses across the cercus coming from any direction in the horizontal plane, allowing us to vary the direction of stimuli given to these four areas independently. Stimulus-evoked responses of cercal INs were recorded using multiple extracellular wire electrodes placed along the ventral nerve cord. Subsequent analysis using the linear array of recording electrodes allowed discrimination of INs by conduction velocity as well as by spike waveform as described in the Methods.

Figure 1B illustrates the discrimination of the extracellular waveforms of 10-2 and 10-3. Although the waveforms in the top red channel appear to come from a single unit, comparison to four channels of a phase-lagged template (thick lines in the five traces) shows otherwise. Specifically, the first and third spikes show similar conduction velocities, whereas the middle

spike had a lower conduction speed. Once these units were separated, IN identity was assigned according to the known tuning properties of these INs.

Figure 2 shows directional tuning curves for L10-2 and L10-3, determined independently for sets of stimuli directed at the bases (blue plots) and tips (red plots) of the cerci. The blue plots show the responses of these two INs to unidirectional air current pulses presented simultaneously to the bases of both cerci, with a maximum amplitude of 8.3 +/-1.2 mm/s at the cercal canopy. The angles labeled on the polar plots indicate the direction in the horizontal plane from which these stimuli were presented to the specimens, with 0° corresponding to stimuli from the front of the animals and 90° to stimuli from the right. Each response was measured as the increase in average firing rate during the 15 ms following the stimulus. The solid blue plots show the mean increase in firing rate, and the blue dashed lines indicate +/- one standard deviation of the firing rate increase across all trials in three animals. All measurements were normalized to the maximum value obtained across all stimulus directions. Unity, or no change in response, is shown by the innermost dashed black circle in each plot grid. Note that these blue polar plots are very similar to plots reported in previous studies for these cells elicited in response to bulk airflow stimulation (Jacobs and Miller, 1983; Miller et al., 1991).

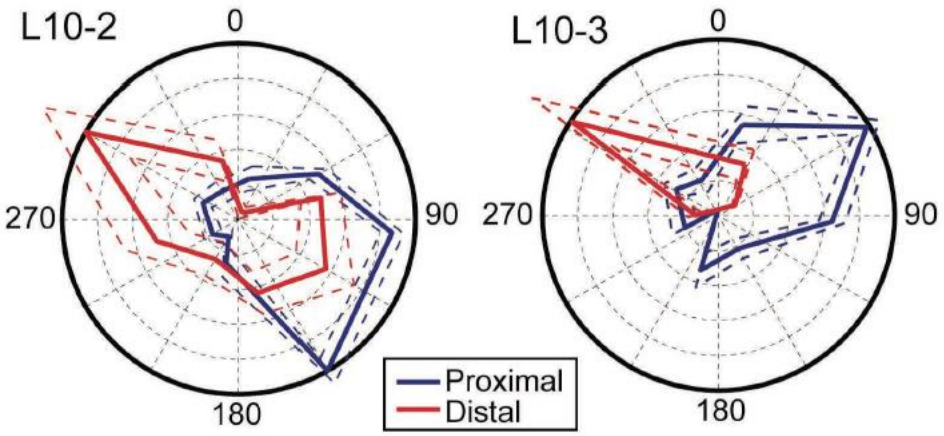

Figure 3.2. Differential spatial and temporal sensitivity of cercal INs. Polar plots of the responses of INs L10-2 and L10-3 respectively. 0° corresponds to stimuli from the front of the animals, and 90° corresponds to stimuli from the right. All responses are plotted as the increase in average firing rate during the 15ms following the stimulus, with all measurements normalized to the maximum value obtained across all stimulus directions for that set of measurements. The outer solid circular axis corresponds to 100% of the maximum response. Red plots show the normalized response to stimuli directed just at the tips of the two cerci. Blue plots show the normalized responses to stimuli at the cercal bases. Solid lines show mean increases in firing rate, dashed lines indicate +/- one standard deviation. The red plots are directional tuning curves for the INs elicited in response to stimulation at the tips of the cerci rather than their bases. Note that the recordings at the tips and bases were normalized independently. The maximum firing rate obtained for base stimulation was 1.36 +/- 0.25 times greater than the maximum rate obtained for tip stimulation in IN 10-2 (1.62 +/- 0.23 in IN 10-3).

It is clear from these results that the INs show different directional selectivity characteristics in response to selective activation of different spatial regions of the cerci. The red tuning curves show maximal sensitivity for stimuli directed at the cercal tips to be shifted 180° (10-2) and 90° (10-3) to the blue curves recorded for stimuli directed at the bases. These results are consistent with earlier electrophysiological and anatomical studies (Jacobs and Miller, 1983; Miller et al., 2011).

Optimal Sets of Simultaneous Multi-Directional Air-Current Stimuli

Having demonstrated that these INs showed differential sensitivity to the local directions of stimuli across the cercal array, we searched for the configuration of four simultaneous air jet stimuli that elicited the largest responses from each of these two different types of INs. To do so, the responses of 10-2 and 10-3 were measured in response to a set of 118 unique stimuli presented to a sample set of five different animals. Each stimulus consisted of a set of four air-pulse jets delivered to the specimen simultaneously, but with each of the four pulses having an independently controlled local direction at each of the four cercal locations (the left tip, left base, right tip, and right base). Each stimulus set of four pulses was presented twenty-five times, shuffled randomly to prevent adaptation. Eight of these 118 stimuli were repeated across all test animals to determine the degree of inter-animal variability. For these eight stimulus sets, the response variability between animals was found to be equivalent to the response variability shown by a single animal to repeats of the same stimulus. Responses were thus pooled and normalized across animals for this set of measurements.

Panels A and B of Figure 3 show the responses of 10-2 to two out of the 118 different stimulus sets. These are raster plots of 10-2's responses, where each row was elicited by a single presentation of the stimulus at time zero (indicated by the purple line on the histogram below the raster plot), and each colored dot represents the time or occurrence of an individual spike. A histogram of each dataset is shown below the raster plot, binned at 3 ms. Panel A corresponds to the previously measured "best" stimulus for L10-2 under bulk airflow conditions: 135° (Miller et al., 1991). Note that the response of this IN to this set of four air jet stimuli was not significantly above baseline. Panel B shows the results for a stimulus set with the same amplitudes but

presented from four different angles: left proximal cercus: 135°, right proximal cercus: 135°, left distal cercus: 210°, right distal cercus: 90°. It is clear that the multi-directional stimulus set delivered in association with panel B elicited a larger and more phase-locked response than the bulk-flow stimulus represented in panel A.

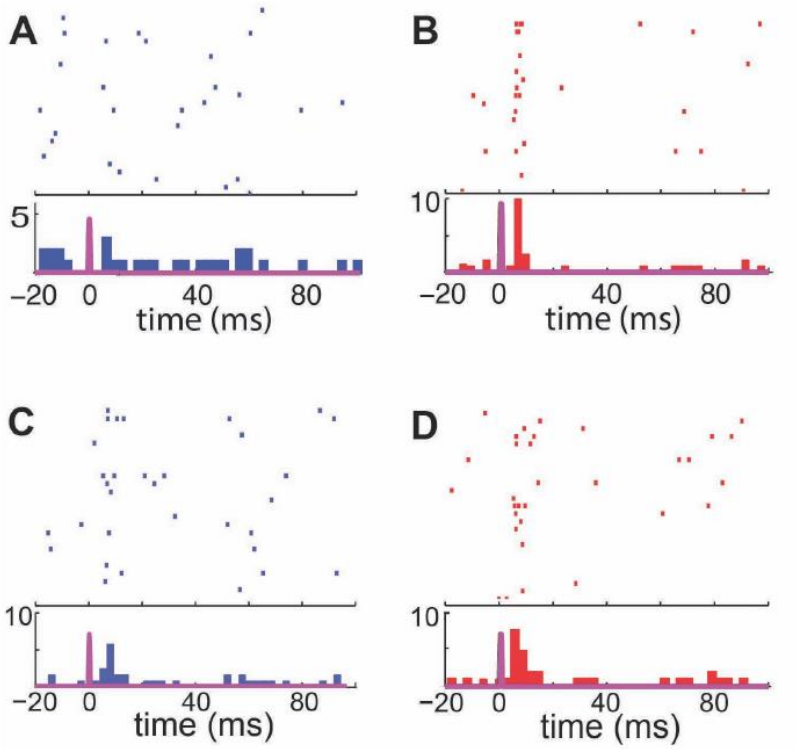

Figure 3.3. Responses of the INs to different sets of 4-jet stimuli. Each panel shows a raster plot of spike times elicited in response to 25 presentations of a 4- jet stimulus pattern, with each colored dot representing the time of occurrence of a single spike. Histograms of the datasets are shown below the corresponding raster plots, binned at 3ms. For all measurements, the 4 stimulus pulses were delivered simultaneously at time zero, indicated by the purple pulse in the histograms. (A) IN L10-2, all 4 stimuli at 135°. (B) IN L10-2, left proximal cercus: 135°, right proximal cercus: 135°, left distal cercus: 210°, right distal cercus: 90° (C) IN L 10-3, all 4 stimuli at 45°. (D) IN L 10-3, Left proximal cercus: 45°, right proximal cercus: 45°, left distal cercus: 200°, right distal cercus: 215°.

Similar data for L10-3 are shown in panels C and D of Figure 3. Responses to a simultaneous four-pulse stimulus corresponding to the previously measured “best” bulk flow stimulus angle (45°) are shown in panel C. Panel D shows the results for a stimulus set with the same

amplitudes but presented from four different angles: left proximal cercus: 45°, right proximal cercus: 45°, left distal cercus: 200°, right distal cercus: 215°. Here again, as was the case for 10-2, the multidirectional stimulus set delivered in association with panel D elicited a larger and more phase-locked response than the bulk-flow stimulus represented by pane C.

We note that the peak amplitudes of the four-pulse stimuli used for the sets of measurements in Figure 3 were substantially lower than those used in earlier experimental studies aimed at characterizing the optimal responses of these two INs with unidirectional bulk air flow stimuli (Jacobs and Miller, 1983; Miller et al., 1991; Theunissen et al., 1996; Theunissen and Miller, 1991). It has been assumed on the basis of those earlier reports that these INs were largely unresponsive to air currents within the low amplitude range used for our multi-directional stimuli. The measurements presented here show that these INs do, in fact, respond in this low-velocity stimulus regime, for particular stimuli having the appropriate small-scale multi-directional structure.

A representation of the general trends of the complete data set from which the panels for Figure 3 were drawn is presented in Figure 4. These panels plot the responses of the INs to repeated presentations of air-pulse stimuli through the four different nozzles. The X axis for each panel is the angle from which one of the four stimuli was directed at the indicated region of the left cercus. The Y axis for each panel is the angle from which another of the four stimuli was directed at the indicated region of the right cercus. The dashed diagonal line from the lower left corner to the upper right corner of each panel indicates the equi-angle stimulus configurations, i.e., this line corresponds to simultaneous bulk airflow movement over both cerci used for stimuli in earlier studies. Color values of the plotted points show the increase (red) or decrease (blue)

from the baseline firing rate in the first 15 ms after stimulation. Only the points showing significant increases or decreases in firing rate are shown here for visual clarity. The color and size of these individual points show the raw recorded firing rate at specific presented stimuli. Background color indicates the two-dimensional spline fit to the full set of data.

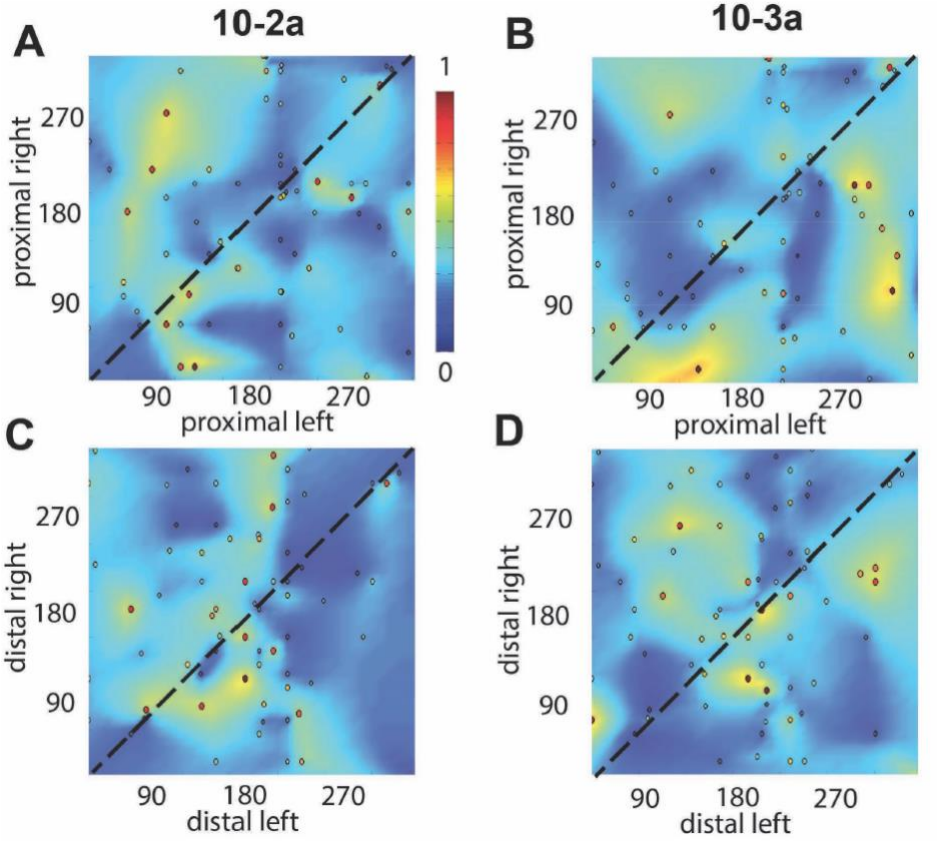

Figure 3.4. Responses of L10-2 and L10-3 to repeated presentations of four independent air-pulse stimuli to different regions of the cerci. X axis for each panel: the angle from which one of the four stimuli was directed at the indicated region of the left cercus. Y axis for each panel: the angle from which another of the four stimuli was directed at the indicated region of the right cercus. The value at each X,Y point in a panel is the average of the responses evoked by all stimuli having those two stimulus directions over the full range of stimulus directions for the other two stimulus jets. See text for details. Color values of the plotted points show the increase (red) or decrease (blue) from the baseline firing rate in the first 15ms after stimulation. Only the points showing significant increases or decreases in firing rate are shown here for visual clarity. Background color indicates the two-dimensional spline fit to the full set of data.

These plots are, by necessity, dimensional reductions of the full stimulus-response data set. Because the four different nozzles could be oriented at the cerci from different direction, a complete specification of the angles for each stimulus-response measurement would require a five-dimensional plot: four dimensions for the stimulus angles and an additional dimension to represent the response amplitude. The representation shown in Figure 4 uses two 3-dimensional panels (X, Y and color) for the data set from each IN, by reducing two stimulus dimensions at each point to an average value over a specific range, as follows. Consider the red point near the upper left corner in panel A of Figure 4. This point represents the average response of L10-2 to all stimulus presentations for which the proximal air jet nozzle over the left cercus was oriented at 90° and the proximal air jet nozzle over the right cercus was oriented at 270°. Only the proximal nozzle angles were constrained for this point in the response space: the data range for the plotted value at this point includes all possible combinations of nozzle angles for the distal air jets. Thus, this point does not correspond to the IN's response to a specific configuration of the four nozzle angles, but rather indicates the trends of the IN's responsiveness to all combinations of four simultaneous air jet pulses that include two pulses to proximal locations at 90° and 270° to the left and right proximal cerci, respectively. This point is in a region that is at a "hotter" color (yellow) than the mean level (green). Thus, air-jet configurations that include stimuli at these two specific angles yield responses that, on average, are above the baseline firing rate of the IN. Correspondingly, air-jet configurations that include stimuli at angles in the "cooler" (blue) regions (e.g., at 180° and 55° to the left and right proximal cerci) yield responses that, on average, are below the baseline firing rate of the IN. This averaging dilutes the significance of the distal configurations and gives a better dependent measure for the two-dimensional

independent variable at the proximal cercal regions. Panel B of Figure 4 shows the corresponding data for L10-3. Panels C (L10-2) and D (L10-3) show the data for stimulation at the distal segments of the left (x-axis) and right (y-axis) cerci.

There are three significant features to note from these plots. First, these stimulus/response terrains are extremely complex, with multiple peaks of responsiveness rather than single-modal distributions. The implicit assumption in earlier studies using bulk-flow stimuli was that the stimulus/response terrain for each IN was a single-modal distribution approximated by a truncated sine function. Second, very few of these response peaks (i.e., a very small fraction of the excitatory responsiveness of the INs) are situated along the equi-angle diagonals of the panels. Note that all the unidirectional bulk stimuli used in previous studies would appear in these panels to lie along the dashed diagonal lines from the lower left to the upper right of each panel. Off-diagonal peaks in the panels of Figure 4 correspond to stimuli for which the jets are directed at the cerci simultaneously from different angles. Third, the proximal and distal maps for each IN are not superimposable, indicating that there are few combinations of 4-jet stimuli for which the optimal pair of (presumably disparate) proximal angles is the same as the optimal pair of (presumably disparate) distal angles.

Differential Sensitivity to Non-Simultaneous Multidirectional Air-Current Stimuli

The preceding experiments demonstrate that the INs had differential sensitivity to simultaneous stimuli presented from different directions at different positions along the cerci. However, most behaviorally-relevant air-current stimuli would be expected to have even more complexity than these multi-directional stimuli. Specifically, such behaviorally important stimuli would have complexity in the time domain, as well as in the spatial domain. Examples of such stimuli

include small recirculating vortex-like stimuli that would impose different directional forcing vectors simultaneously and/or sequentially at different positions along the cerci (Heinzel and Dambach, 1987; Kamper and Dambach, 1981) and discrete air-current wavefronts that sweep along the cerci (Casas et al., 2008; Casas and Dangles, 2010; Casas and Steinmann, 2014; Comer et al., 1994; Dangles et al., 2009, 2006; Dupuy et al., 2012; Gnatzy and Heusslein, 1986; Gnatzy and Kamper, 1990; Magal et al., 2006). Therefore, we carried out additional experiments to determine if the INs displayed differential sensitivity to multidirectional stimulus pulses that were not simultaneous. To test for this sensitivity, we used the same four-nozzle stimulus apparatus described above to generate stimuli from up to four different directions and varied the timing between the stimulus pulses. It was beyond the scope of this study to do an exhaustive determination of the stimulus-response characteristics of both INs to all possible combinations of intervals between the four multi-directional stimulus pulses.

Instead, we limited our measurements to the responses of L10-2 to inter-stimulus pulse intervals of 5ms.

Figure 5 presents a dimensionally-reduced representation of the stimulus response dataset for IN 10-2 to non-simultaneous multi-directional air current stimuli. This representation is a set of nine response surfaces. The format for each of these plots is the same as that used in Figure 4, but without the dashed diagonal line indicating the equiangle stimulus contour. The small “x” symbols are the locations within the stimulus space at which the recorded data showed significant increases or decreases in firing rate from the average baseline activity levels. For clarity, the axis labels are only indicated for the lower left panel (Figure 5G). Labels for all other panels are identical to those for panel G. The data for the center panel (Figure 5E) is identical to

that for Figure 4A. This panel, Figure 5E, shows the averaged responses of 10-2 when the four stimuli were delivered to all parts of cercal array at the same time. To reiterate the plotting scheme, each point in Figure 5E represents the average response of 10-2 to all stimulus presentations for which the proximal air jet nozzle over the left cercus was oriented at the value indicated on the X axis, and the proximal air jet nozzle over the right cercus was oriented at the value indicated on the Y axis, averaged over all possible combinations of nozzle angles for the distal air jets.

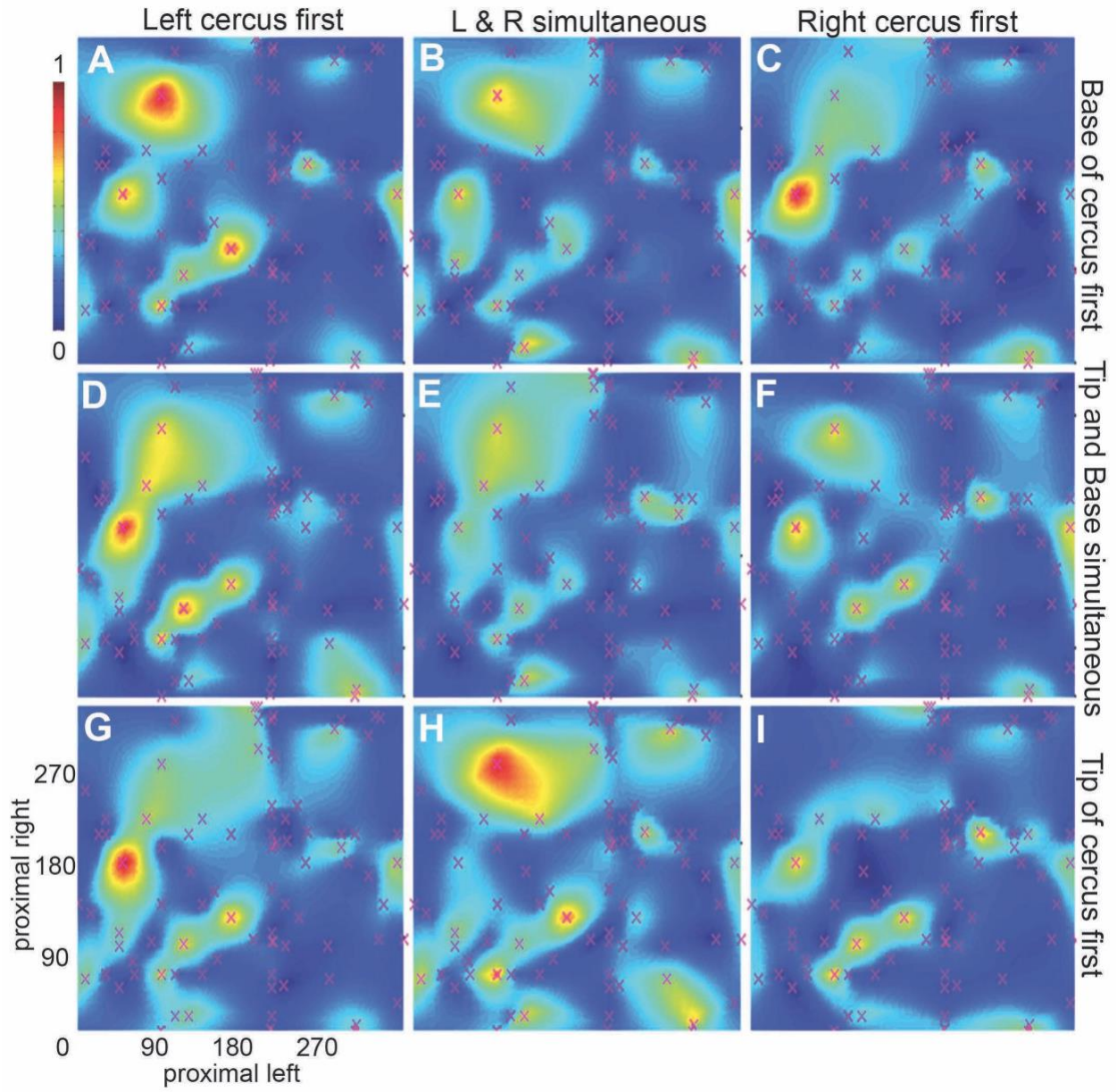

Figure 3.5. Responses of L10-2 to repeated presentations of four independent air-pulse stimuli with different latencies to different regions of the cerci. Each panel corresponds to a different combination of delay intervals between stimuli to different cercal regions. X axis for each panel: the angle from which one of the four stimuli was directed at the proximal left cercus. Y axis for each panel: the angle from which another of the four stimuli was directed at the proximal right cercus. The value at each X,Y point in a panel is the average of the responses evoked by all stimuli having those two stimulus directions over the full range of stimulus directions for the other two stimulus jets onto the distal cerci. Color values show the increase (red) or decrease (blue) from the baseline firing rate in the first 15ms after stimulation. Background color indicates the two-dimensional spline fit to the full set of data. Only the points showing significant increases or decreases in firing rate are shown here for visual clarity. Values in all panels were scaled to the

global maximum value across all measurements in all panels. (E) This panel is equivalent to Figure 4A and is the basis for comparison for the other panels. It shows the averaged responses of 10-2 when the four stimuli were delivered to all parts of cercal array at the same time. (B) Averaged responses when two air jet stimuli were delivered to the base of the cerci 5ms before the two other air jet stimuli in the set of four were delivered to the tips of the cerci. (H) Averaged response when the tips were stimulated 5ms before the bases. (D) Averaged responses when the left cercus was stimulated 5ms before the right cercus. (F) Averaged responses when the right cercus was stimulated 5ms before the left cercus. The four corner panels (A,C,G,I) correspond to diagonal sweeps of the stimuli across the cerci. (A) Averaged responses when a single stimulus is applied to the base of the left cercus, followed 5ms later by stimuli to the tip of the left cercus and the base of right cercus, followed 5ms later by a stimulus to the tip of the right cercus. (C) Averaged responses when a single stimulus is applied to the base of the right cercus, followed 5ms later by stimuli to the tip of the right cercus and the base of left cercus, followed 5ms later by a stimulus to the tip of the left cercus. (G) Averaged responses when a single stimulus is applied to the tip of the left cercus, followed 5ms later by stimuli to the base of the left cercus and the tip of right cercus, followed 5ms later by a stimulus to the base of the right cercus. (I) Averaged responses when a single stimulus is applied to the tip of the right cercus, followed 5ms later by stimuli to the base of the right cercus and the tip of left cercus, followed 5ms later by a stimulus to the base of the left cercus.

All other surrounding panels in Figure 5 correspond to responses evoked from this IN when the timings between pulses to the different regions of the cerci were varied by 5 ms intervals. The different stimulus regimes are indicated in the labels above the three columns and to the right of the tree rows. The three panels in the left column correspond to all cases where the stimulus pulses were delivered to the left cercus region 5 ms before the pulses were delivered to the right cercus region. The center column corresponds to cases where the pulses were delivered simultaneously to the indicated regions, and the rightmost column of three panels corresponds to the cases where the stimuli to the indicated regions to the right cercus preceded those to the left. In contrast, the top row of three panels corresponds to cases where the stimuli to the bases of the indicated cerci preceded those to the tips by 5 ms, etc.

To illustrate, consider several specific panels of this figure. Figure 5B, immediately above panel E, shows the averaged response surface when two air jet stimuli were delivered to the base of the

cerci 5 ms before the two other air jet stimuli in the set of four were delivered to the tips of the cerci. Panel 5H, directly below panel 5E, shows the IN's averaged response when the tips were stimulated 5 ms before the bases. Similarly, panel 5D shows the responses when the left cercus was stimulated 5 ms before the right cercus, and panel 5F shows the responses when the right cercus was stimulated 5 ms before the left cercus. The four corner panels (A, C, G, I) correspond to diagonal sweeps of the stimuli across the cerci. For example, panel 5A corresponds to a single stimulus applied to the base of the left cercus, followed 5 ms later by stimuli to the tip of the left cercus and the base of right cercus. Values in all panels were scaled to the global maximum value across all measurements in all panels.

The most significant feature to note from these panels is that there are nonsynchronous, multi-directional stimuli which are much more effective at eliciting responses from 10-2 than any previously studied synchronous unidirectional (bulk-flow) stimuli, or synchronous multi-directional stimuli shown in the preceding figures. Note that the previously studied bulk-flow stimuli to 10-2 are represented only along the diagonal of the central panel 5E, and all synchronous multidirectional stimuli are represented by the off-diagonal regions of panel 5E. For the subset of the stimulus-response space represented here, the largest responses were elicited in panel 5H by off-axis (i.e., multi-direction) stimuli arriving at the tips of the cerci 5 ms before those at the base. There were several other non-synchronous, multi-directional stimuli sets that also gave much larger responses than those in panel 5E (in panels A, C, D and G).

Neuroanatomical Basis for Differential Sensitivity to Non-Simultaneous Multi-Directional Air-Current Stimuli

Previous studies by Jacobs and colleagues have yielded a three-dimensional atlas of the sensory afferent map within the terminal abdominal ganglion, based on an extensive set of detailed anatomical reconstructions of the sensory afferent synaptic arborizations (Jacobs and Theunissen, 1996; Paydar et al., 1999; Troyer et al., 1994). Jacobs and colleagues have also used that probabilistic atlas to estimate and visualize the mapping of cercal sensory receptor afferents onto the dendrites of cercal interneurons (Cummins et al., 2003; Jacobs and Pittendrigh, 2002; Jacobs and Theunissen, 2000). Figure 6 shows the results of using this probabilistic atlas to visualize the overlap of cercal sensory afferents onto the dendrites of interneurons L10-2 and L10-3, in a manner that yields insights into their sensitivity to small-scale multi-directional inputs.

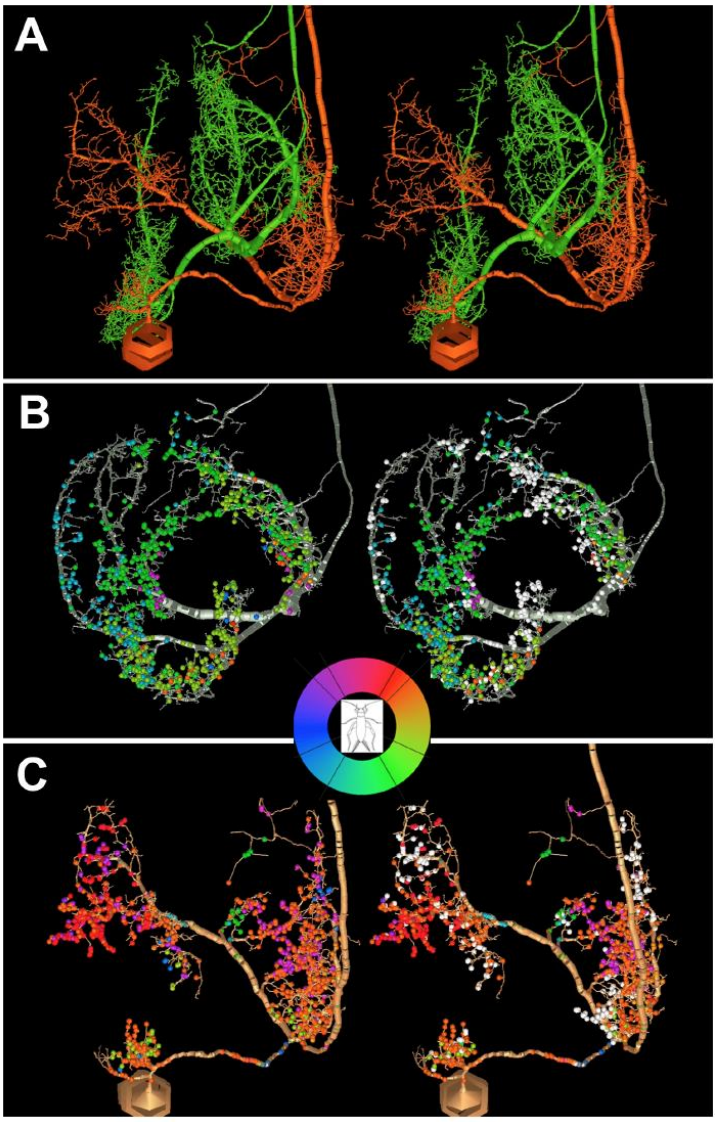

Figure 3.6. Reconstructions of INs L10-2 and L10-3. (A) Stereo pair of anatomical reconstructions of L10-2 and L10-3, normalized to their relative positions as they would be viewed from the dorsal surface of the terminal abdominal ganglion. Each IN is colored according to its peak directional selectivity as measured in previous studies using bulk airflow stimuli. The key for this color scheme (and for all other panels) is shown in the circular form between panels B and C. (B) L10-2, reoriented with respect to panel A in a manner to allow best visualization of the dendritic branches. This pair of images is also a stereo pair, but the two panels have a different coloring scheme. The image on the left side of panel B shows the result of masking the afferent map of afferent synaptic terminals onto the dendrites of L10-2. Each small colored dot represents an intersection of the IN's dendritic branch with a region of the cercal glomerulus that contains afferent synaptic terminals. The color of each small dot indicates the directional selectivity of the afferent receptors having synaptic terminals in that region of the atlas. The right image in panel B is a transformation of the image in the left panel: in the right image, all of the spheres associated with inputs from sensory hairs on the distal half of the cerci have been colored white, and the

spheres associated with sensory hairs on the proximal cerci remain with their original colors. (C) IN L10-3, presented in the same format as IN10-2 in panel B. The image on the left side of panel C shows the result of masking the afferent map of afferent synaptic terminals onto the dendrites of L10-3. In the right image of panel C, all the spheres associated with inputs from sensory hairs on the distal half of the cerci have been colored white, and the spheres associated with sensory hairs on the proximal cerci remain with their original colors.

Panel 6A is a stereo pair of anatomical reconstructions of L10-2 and L10-3, normalized to their relative positions as they would be viewed from the dorsal surface of the terminal abdominal ganglion. Each IN is colored according to its peak directional selectivity as measured in previous studies using bulk-airflow stimuli. The key for this color scheme (and for all other panels of Figure 6) is shown in the circle between panels B and C. L10-2 is maximally responsive to bulk flow stimuli from the right rear region centered at 135° and is therefore colored green. Note that 10-2's cell body removed from the image so that it does not obscure visibility of any dendrites. L10-3 is maximally responsive to bulk flow stimuli from the right front region centered at 45° and is therefore colored orange.

Panel 6B shows the structure of 10-2, reoriented with respect to panel A in a manner to allow best visualization of the dendritic branches. This pair of images is also a stereo pair, but the two panels have a different coloring scheme in order to highlight one important aspect of the afferent synaptic innervation pattern. The image on the left side of Figure 6B shows the result of masking the afferent map of afferent synaptic terminals onto the dendrites of L10-2. Each small colored dot represents an intersection of the IN's dendritic branch with a region of the cercal glomerulus that contains afferent synaptic terminals. The color of each small dot indicates the directional selectivity of the afferent receptors having synaptic terminals in that region of the atlas. The color of the dots onto 10-2 are predominantly green, indicating that the predominant synaptic

inputs are from afferents activated by air currents from the right rear of the cricket (approximately 135°). This is consistent with earlier observations of the directional selectivity of L10-2 to bulk-airflow stimuli (Miller et al., 1991), and with the results presented in Figure 2A above. It is also important to note from the left image in Panel 6B that there are many dendritic regions that are situated in regions where synaptic inputs are from afferents activated by air currents from a variety of other directions, including the diametrical opposite of the optimal direction for bulk flow stimuli. This is also consistent with the results presented in Figure 2A above.

The right image in Figure 6B is a transformation of the image in the left panel of 6B: in this right panel, all the spheres associated with inputs from sensory hairs on the distal half of the cerci have been colored white, and the spheres associated with sensory hairs on the proximal cerci remain with their original colors. By comparing the left and right panels of Figure 6B, three significant features can be noted. First, the majority of the spheres that are innervated by distal hairs were light green, indicating a predominance of distal input from 115°, though there were also a significant number of distal inputs associated with blue dots (i.e., inputs sensitive to air currents from approximately 240°). Second, the inputs from distal sensory hairs appear to be clustered in groups, rather than randomly distributed across the dendritic branches. Third, those input clusters from distal hair groups were located at distal regions of the dendrites. All of these features would be expected to support differential selectivity to multi-directional, temporally sequenced stimuli to this IN, as discussed below.

Panel 6C shows equivalent data for L10-3. The same general conclusions can be drawn for this IN as for 10-2. The color of the dots onto 10-3 are predominantly orange, indicating that the

predominant synaptic inputs are from afferents activated by air currents from the right front of the cricket (approximately 45°). This is consistent with earlier observations of the directional selectivity of IN L10-3 to bulk-airflow stimuli [2,3], and with the results presented in Figure 2B. As was the case for 10-2 in panel 6B, Panel 6C also shows that there are many dendritic regions in 10-3 that are situated in regions where synaptic inputs are from afferents activated by air currents from a variety of other directions, including those from the left front of the animal (color coded as purple). This is also consistent with the results presented in Figure 2B.

In the right image of panel 6C, all the spheres associated with inputs onto L10-3 from sensory hairs on the distal half of the cerci have been colored white, and the spheres associated with sensory hairs on the proximal cerci remain with their original colors. By comparing the left and right images of 6C, the same general conclusions can be drawn as for 10-2. For 10-3, most of the spheres that are innervated by distal hairs were from inputs with different directional selectivity than those from the predominant (orange-colored) inputs. As was the case for 10-2, the inputs from distal sensory hairs onto 10-3 appear to be clustered in groups, and those input clusters from distal hair groups were located at distal regions of the dendrites. Here again, all these features would be expected to support to differential selectivity to air currents with complex spatiotemporal structure.

Discussion

We demonstrate here that four primary cercal sensory interneurons respond with high sensitivity to complex dynamic multi-directional features of air currents that have spatial scales smaller than the physical dimensions of the cerci. The velocity threshold for these features is substantially lower than the threshold for simple large-scale unidirectional bulk-flow stimuli used in previous

studies. Thus, these four cells are responding in a manner that would be consistent with their functioning as feature detectors for stimuli corresponding to naturalistic stimuli such as approaching predators, competitors or mates. We do not suggest that the responsiveness to unidirectional bulk-flow stimuli documented in previous studies is spurious or artifactual; rather, we demonstrate here that as well as responding to higher-velocity bulk flow stimuli, the cercal system is also capable of responding reliably to more complex stimuli with lower amplitudes than were used in those previous studies. In this sense, these INs are theoretically capable of multiplexing information about their stimulus environment: the ratios of the ongoing mean spike rates encode the bulk air movement drift around the animals, and very brief bursts of spikes like the ones shown in Figure 3 indicate the detection of a behaviorally relevant feature. This is consistent with studies demonstrating that INs 10-2 and 10-3 are capable of using temporal patterns of spikes as fundamental symbols in their neural code (Aldworth et al., 2011).

Figure 5 shows the extreme spatial and temporal complexity of the stimulus-response space for one of the INs studied here: L10-2. The largest response recorded from this IN, shown in panel 5H, was elicited by a set of four stimulus puffs that originated from four different directions, with the two stimuli to the cercal tips arriving 5ms before those at the base of the cerci. There were several more stimulus sets with other combinations of directions and delays that were almost as effective. It is important to note that the best stimulus seen in panel H of Figure 5 is not necessarily the globally optimal stimulus for IN 10-2. In order to determine the global optimum, if such an optimum exists, an extremely exhaustive set of measurements would need to be taken, using a much wider and more finely parsed range of relative delay intervals, and having finer

angular separations between the air nozzles. Such a set of measurements was beyond the scope of this study.

It would be interesting and enlightening to determine if such an optimum stimulus exists for this (or any other) IN, for several reasons. If a single optimum exists and is considerably more effective at eliciting a response than even any of the stimuli tested here, then the IN could presumably be thought of as a feature detector. Although the set stimulus parameters could not be "inverted", in the strict mathematical sense, to derive the precise identity of the stimulus (e.g., charging spider or approaching mate), the general nature of the stimulus set might be used as a way to screen between a possible set of stimulus sources, or to serve as a standard for comparison of air currents recorded from putative sources such as those studied by Casas and colleagues (Casas et al., 2008). It is perhaps more likely that an exhaustive characterization of the response space would present a complex terrain with several or many peaks. In that case, a thoughtful analysis of that terrain might yield a deeper understanding of the IN's role in the system's operation. For example, all response peaks might correspond to objects approaching from a particular range of directions within a particular range of speeds.

Physiological and Anatomical Basis for the Observed Complex Sensitivities

Several factors may contribute to the observed spatiotemporal complexity of the INs' stimulus/response properties. The most likely are 1) the selective synaptic connectivity with subsets of the sensory afferents (Bacon and Murphey, 1984; Cummins et al., 2003; Jacobs and Miller, 1983; Jacobs and Pittendrigh, 2002; Jacobs and Theunissen, 2000), 2) the passive internal filtering of those synaptic inputs due to the electrotonic structure of the dendrites (Jacobs and

Miller, 1985; Miller and Jacobs, 1984), 3) any active transformations of the synaptic currents due to voltage dependent conductance mechanisms in the dendrites (Ogawa et al., 2008, 2006, 2004, 2002a, 2002b, 2001, 2000, 1999, 1996), 4) and the inter-neuronal synaptic circuitry mediated by local interneurons (Baba et al., 1995, 1991; Bodnar, 1993; Bodnar et al., 1991). The experiments reported here could not yield any insights into the involvement of the latter two mechanisms. However, the results are clearly interpretable within the first two mechanistic realms.

Selective Synaptic Connectivity with Subsets of the Sensory Afferents

Previous research has demonstrated how the selective connectivity between cercal INs and specific subsets of sensory afferents is a major determinant of the directional selectivity of the INs to bulk air flow stimuli. Electrophysiological studies showed that IN tuning curves to bulk air flow stimuli emerged from averages of the responses of sensory receptors that had different directional selectivities, and that the overall net tuning curves were biased toward the responses elicited from the more dense populations of sensory hairs near the bases of the cerci (Jacobs and Miller, 1983). Several other anatomical studies have documented the complex manner with which the directional selectivity of sensory hairs varies as a function of the position on the cerci (Bacon and Murphey, 1984; Miller et al., 2011). The results presented here support those earlier conclusions but extend our insights about the INs' responsiveness into a different stimulus regime, by eliminating the *de facto* spatial and temporal averaging imposed by the use of bulk-flow stimuli. Specifically, we demonstrate that the presence of afferents of different directional selectivities onto the IN dendrites, originating from receptors located on different regions of the cerci, support differential sensitivity of the INs to stimuli that have multiple directional components within a spatial scale smaller than the dimensions of the cerci. In other words, the

spatiotemporal averaging imposed by our previous use of bulk flow stimuli made it impossible to detect aspects of the IN responsiveness which would support their operation as feature detectors.

Electrotonic Structure of the IN Dendrites

Earlier research has shown that the primary determinant of selective connectivity between an IN and its specific subset of sensory receptor afferent inputs is the dendritic structure of the INs: the position of an IN's dendrites within the afferent map determines the subset of afferents with which it may come into contact (Bacon and Murphey, 1984; Cummins et al., 2003; Jacobs and Miller, 1983; Jacobs and Pittendrigh, 2002; Jacobs and Theunissen, 2000). Modeling studies based on accurate reconstructions of the IN 10-3 supported the conclusions drawn from studies using bulk-airflow stimuli and were able predict the directional tuning of the IN (Cummins et al., 2003; Jacobs and Pittendrigh, 2002; Jacobs and Theunissen, 2000). But as in the other earlier studies mentioned above, no considerations were given to stimuli with complex spatiotemporal structures like the ones used in the experiments reported here. Although a modeling study was beyond the scope of our experiments, a qualitative consideration of the dendritic structure of these INs yields insights into aspects of their electrotonic characteristics that could support their observed feature sensitivities.

Figure 6 shows that the afferent synaptic inputs onto the IN dendrites tended to be segregated into groups with respect to two attributes: 1) the directional specificity of the afferents, and 2) the location of the afferents out along the cerci. The second factor has not been noted or considered in previous studies and could be of considerable significance. We demonstrated recently that spikes arriving at the terminal abdominal ganglion from distal cercal mechanoreceptors have a significantly greater latency than spikes arriving from more proximal receptors, due to the added

conduction time along the length of the cercus (Chapter 2; Mulder-Rosi et al., 2010). The temporal latency was measured to be up to 5 ms. This means that the action potentials arriving at synapses indicated with the white spheres in Figure 6 will have had conduction times up to 5 ms greater than those APs arriving at the other (colored) sites. This non-uniform distribution of synaptic inputs from the distal cercal afferents onto the IN dendrites, in combination with the delay-line characteristics of the cerci, could support substantial differential sensitivity of an IN to small-scale, multi-directional naturalistic stimuli sweeping over the cerci at different velocities. For example, the production of a burst of afferent synaptic input that would simultaneously activate the entire extent of the dendritic branches of each IN would require a very specific set of directional air currents oriented along the cerci, sequenced in time with latencies of up to 5 ms. First order predictions of an optimal multi-jet stimulus could be derived from a quantitative analysis of the data shown in Fig 6 and used as a starting point in a more exhaustive search for such globally optimal stimuli.

Acknowledgements

We thank Gwen Jacobs for use of her anatomical reconstruction database and for helpful discussions and comments. We thank Graham Cummins for software development and support. We thank Susan Krueger for expert technical assistance with lab procedures.

References

Aldworth, Z.N., Dimitrov, A.G., Cummins, G.I., Gedeon, T., Miller, J.P., 2011. Temporal encoding in a nervous system. PLoS Comput Biol 7, e1002041. https://doi.org/10.1371/journal.pcbi.1002041

Baba, Y., Hirota, K., Yamaguchi, 1991. Morphology and response properties of wind-sensitive non-giant interneurons in the terminal abdominal ganglion of crickets. Zoological Science 8, 437–445.

Baba, Y., Hirota, K., Yamaguchi, T., Shimozawa, T., 1995. Differing afferent connections of spiking and nonspiking wind-sensitive local interneurons in the terminal abdominal ganglion of the cricket Gryllus bimaculatus. J Comp Physiol A 176. https://doi.org/10.1007/BF00197749

Bacon, J.P., Murphey, R.K., 1984. Receptive fields of cricket giant interneurones are related to their dendritic structure. The Journal of Physiology 352, 601–623. https://doi.org/10.1113/jphysiol.1984.sp015312

Bodnar, D.A., 1993. Excitatory influence of wind-sensitive local interneurons on an ascending interneuron in the cricket cercal sensory system. J Comp Physiol A 172, 641–651. https://doi.org/10.1007/BF00213686

Bodnar, DeanaA., Miller, JohnP., Jacobs, GwenA., 1991. Anatomy and physiology of identified wind-sensitive local interneurons in the cricket cercal sensory system. J Comp Physiol A 168, 553–564. https://doi.org/10.1007/BF00215077

Butts, D.A., Goldman, M.S., 2006. Tuning curves, neuronal variability, and sensory coding. PLoS Biol 4, e92. https://doi.org/10.1371/journal.pbio.0040092

Casas, J., Dangles, O., 2010. Physical Ecology of Fluid Flow Sensing in Arthropods. Annu. Rev. Entomol. 55, 505–520. https://doi.org/10.1146/annurev-ento-112408-085342

Casas, J., Steinmann, T., 2014. Predator-induced flow disturbances alert prey, from the onset of an attack. Proc. R. Soc. B. 281, 20141083. https://doi.org/10.1098/rspb.2014.1083

Casas, J., Steinmann, T., Dangles, O., 2008. The aerodynamic signature of running spiders. PLoS ONE 3, e2116. https://doi.org/10.1371/journal.pone.0002116

Comer, C., Mara, E., Murphey, K., Getman, M., Mungy, M., 1994. Multisensory control of escape in the cockroach Periplaneta americana. Journal of Comparative Physiology A 174, 13–26.

Cummins, B., Gedeon, T., Klapper, I., Cortez, R., 2007. Interaction between arthropod filiform hairs in a fluid environment. Journal of Theoretical Biology 247, 266–280. https://doi.org/10.1016/j.jtbi.2007.02.003

Cummins, G.I., Crook, S.M., Dimitrov, A.G., Ganje, T., Jacobs, G.A., Miller, J.P., 2003. Structural and biophysical mechanisms underlying dynamic sensitivity of primary sensory interneurons in the cricket cercal sensory system. Neurocomputing 52–54, 45–52. https://doi.org/10.1016/S0925-2312(02)00786-5

Dangles, O., Casas, J., Coolen, I., 2006. Textbook cricket goes to the field: the ecological scene of the neuroethological play. Journal of Experimental Biology 209, 393–398. https://doi.org/10.1242/jeb.02000

Dangles, O., Irschick, D., Chittka, L., Casas, J., 2009. Variability in sensory ecology: expanding the bridge between physiology and evolutionary biology. The Quarterly Review of Biology 84, 51–74. https://doi.org/10.1086/596463

Dupuy, F., Steinmann, T., Pierre, D., Christidès, J.-P., Cummins, G., Lazzari, C., Miller, J., Casas, J., 2012. Responses of cricket cercal interneurons to realistic naturalistic stimuli in the field. Journal of Experimental Biology 215, 2382–2389. https://doi.org/10.1242/jeb.067405

Gnatzy, W., Heusslein, R., 1986. Digger wasp against crickets: I. Receptors involved in the antipredator strategies of the prey. Naturwissenschaften 73, 212–215. https://doi.org/10.1007/BF00417728

Gnatzy, W., Kamper, G., 1990. Digger wasp against crickets. II. An airborne signal produced by a running predator. J Comp Physiol A 167. https://doi.org/10.1007/BF00190826

Heinzel, H.-G., Dambach, M., 1987. Travelling air vortex rings as potential communication signals in a cricket. J. Comp. Physiol. 160, 79–88. https://doi.org/10.1007/BF00613443

Huang, Y., Miller, J., 2004. Phased-array processing for spike discrimination. Journal of Neurophysiology 92, 1944–1957.

Jacobs, G., Miller, J., 1985. Functional properties of individual neuronal branches isolated in situ by laser photoinactivation. Science 228, 344–346. https://doi.org/10.1126/science.3983633

Jacobs, G., Miller, J., 1983. Cellular mechanisms underlying directional sensitivity of an identified sensory interneuron. Journal of Neuroscience 6, 2298–2311.

Jacobs, G., Pittendrigh, C., 2002. Predicting emergent properties of neuronal ensembles a database of individual neurons, in: Computational Neuroanatomy. Humana Press, Totowa, NJ, pp. 151–170.

Jacobs, G., Theunissen, F., 1996. Functional organization of a neural map in the cricket cercal sensory system. J. Neurosci. 16, 769–784. https://doi.org/10.1523/JNEUROSCI.16-02-00769.1996

Jacobs, G.A., Miller, J.P., Aldworth, Z., 2008. Computational mechanisms of mechanosensory processing in the cricket. Journal of Experimental Biology 211, 1819–1828. https://doi.org/10.1242/jeb.016402

Jacobs, G.A., Murphey, R.K., 1987. Segmental origins of the cricket giant interneuron system. J. Comp. Neurol. 265, 145–157. https://doi.org/10.1002/cne.902650110

Jacobs, G.A., Theunissen, F.E., 2000. Extraction of sensory parameters from a neural map by primary sensory interneurons. J. Neurosci. 20, 2934–2943. https://doi.org/10.1523/JNEUROSCI.20-08-02934.2000

Kamper, G., Dambach, M., 1981. Response of the cercus-to-giant interneuron system in crickets to species-specific song. J. Comp. Physiol. 141, 311–317. https://doi.org/10.1007/BF00609933

Magal, C., Dangles, O., Caparroy, P., Casas, J., 2006. Hair canopy of cricket sensory system tuned to predator signals. Journal of Theoretical Biology 241, 459–466. https://doi.org/10.1016/j.jtbi.2005.12.009

Miller, J.P., Jacobs, G.A., 1984. Relationships between neuronal structure and function. J Exp Biol 112, 129–145.

Miller, J.P., Jacobs, G.A., Theunissen, F.E., 1991. Representation of sensory information in the cricket cercal sensory system. I. Response properties of the primary interneurons. Journal of Neurophysiology 66, 1680–1689. https://doi.org/10.1152/jn.1991.66.5.1680

Miller, J.P., Krueger, S., Heys, J.J., Gedeon, T., 2011. Quantitative characterization of the filiform mechanosensory hair array on the cricket cercus. PLoS ONE 6, e27873. https://doi.org/10.1371/journal.pone.0027873

Mulder-Rosi, J., Cummins, G.I., Miller, J.P., 2010. The cricket cercal system implements delay-line processing. Journal of Neurophysiology 103, 1823–1832. https://doi.org/10.1152/jn.00875.2009

Ogawa, H., Baba, Y., Oka, K., 2004. Directional sensitivity of dendritic calcium responses to wind stimuli in the cricket giant interneuron. Neuroscience Letters 358, 185–188. https://doi.org/10.1016/j.neulet.2004.01.023

Ogawa, H., Baba, Y., Oka, K., 2002a. Spike-triggered dendritic calcium transients depend on synaptic activity in the cricket giant interneurons. J. Neurobiol. 50, 234–244. https://doi.org/10.1002/neu.10032

Ogawa, H., Baba, Y., Oka, K., 2002b. Direction of action potential propagation influences calcium increases in distal dendrites of the cricket giant interneurons. J. Neurobiol. 53, 44–56. https://doi.org/10.1002/neu.10105

Ogawa, H., Baba, Y., Oka, K., 2001. Dendritic calcium accumulation regulates wind sensitivity via short-term depression at cercal sensory-to-giant interneuron synapses in the cricket. J Neurobiol 46, 301–313.

Ogawa, H., Baba, Y., Oka, K., 2000. Spike-dependent calcium influx in dendrites of the cricket giant interneuron. J. Neurobiol. 44, 45–56. https://doi.org/10.1002/1097-4695(200007)44:1<45::AID-NEU5>3.0.CO;2-#

Ogawa, H., Baba, Y., Oka, K., 1999. Dendritic Ca2+ transient increase evoked by wind stimulus in the cricket giant interneuron. Neuroscience Letters 275, 61–64. https://doi.org/10.1016/S0304-3940(99)00744-2

Ogawa, H., Baba, Y., Oka, K., 1996. Dendritic Ca2+ response in cercal sensory interneurons of the cricket Gryllus bimaculatus. Neuroscience Letters 219, 21–24. https://doi.org/10.1016/S0304-3940(96)13162-1

Ogawa, H., Cummins, G.I., Jacobs, G.A., Miller, J.P., 2006. Visualization of ensemble activity patterns of mechanosensory afferents in the cricket cercal sensory system with calcium imaging. J. Neurobiol. 66, 293–307. https://doi.org/10.1002/neu.20220

Ogawa, H., Cummins, G.I., Jacobs, G.A., Oka, K., 2008. Dendritic design implements algorithm for synaptic extraction of sensory information. Journal of Neuroscience 28, 4592–4603. https://doi.org/10.1523/JNEUROSCI.5354-07.2008

Paydar, S., Doan, C.A., Jacobs, G.A., 1999. Neural mapping of direction and frequency in the cricket cercal sensory system. J. Neurosci. 19, 1771–1781. https://doi.org/10.1523/JNEUROSCI.19-05-01771.1999

Salinas, E., Abbott, L.F., 1994. Vector reconstruction from firing rates. J Comput Neurosci 1, 89–107. https://doi.org/10.1007/BF00962720

Theunissen, F., Roddey, J.C., Stufflebeam, S., Clague, H., Miller, J.P., 1996. Information theoretic analysis of dynamical encoding by four identified primary sensory interneurons

in the cricket cercal system. Journal of Neurophysiology 75, 1345–1364. https://doi.org/10.1152/jn.1996.75.4.1345

Theunissen, F.E., Miller, J.P., 1991. Representation of sensory information in the cricket cercal sensory system. II. Information theoretic calculation of system accuracy and optimal tuning-curve widths of four primary interneurons. Journal of Neurophysiology 66, 1690–1703. https://doi.org/10.1152/jn.1991.66.5.1690

Troyer, T.W., Levin, J.E., Jacobs, G.A., 1994. Construction and analysis of a database representing a neural map. Microsc. Res. Tech. 29, 329–343. https://doi.org/10.1002/jemt.1070290502

CHAPTER FOUR

CONCLUSIONS

In this dissertation, I focus on the nervous system of the cricket *Acheta domesticus*, which has been used as a model system for investigating the mechanisms underlying neural coding at the cellular and system levels for over 40 years. The sense organ for this system is a pair of antenna-like abdominal appendages called cerci. Sensory input from ~750 wind-sensitive mechanosensory hairs along the cerci forms a well-studied spatial map in the cercal glomerulus. A number of projecting interneurons then collect information from these afferents and send forward biologically relevant information. Interneurons in this system are readily identifiable across organisms and show a similar dendritic architecture even when peripheral afferents are missing throughout development. This creates a system where the information available to an interneuron is determined largely by its heritable genetic program and can be easily observed in the cell's morphology.

The cricket's survival can depend on an escape mechanism able to detect the slightest air movements (Casas et al., 2008), such as those produced by an approaching spider, while ignoring wind and self-motion stimuli. Previously, it was assumed that signals from sensory cells in the nervous system of the cricket encoded only information about the *direction* of a moving air stimulus. However, for the response to be effective, the cricket would also require information on the *location* of the threat. In Chapter 2, I show that the differential conduction characteristics of the receptor array in *Acheta domesticus* crickets are of substantial significance. All the filiform sensory afferent axons that I examined had the same propagation speeds to within a small variance, resulting in a significant and systematic differential propagation time for spikes

from sensory receptors at different locations along the structure. Thus, the sensory structures operate as delay-lines.

The delay-line structure supports neural computations in many of the projecting cercal interneurons (INs) that yield substantial differential sensitivity to the direction and velocity of stimuli such as those produced by predators. The air-particle velocity of approaching spiders, for example, has been shown to fall off significantly over several centimeters (Figure 1; Casas et al., 2008). Some spiders take advantage of this nonlinearity and display two foraging modes: an ambush strategy, which reduces the distance at which the prey can perceive the spider, or a high-speed attack that makes the encounter more likely to be faster than the prey's escape response. Several INs in the cercal system show delay-line-derived sensitivities of large importance for survival that are equivalent, in an engineering sense, to “notch filtering”, through which background noise is selectively eliminated by the delay-line-based processing. The existence of this delay line suggests that it is also possible for an incoming neuron to encode the *location* of the wind stimulus along the sensory array of hairs (Mulder-Rosi et al., 2010).

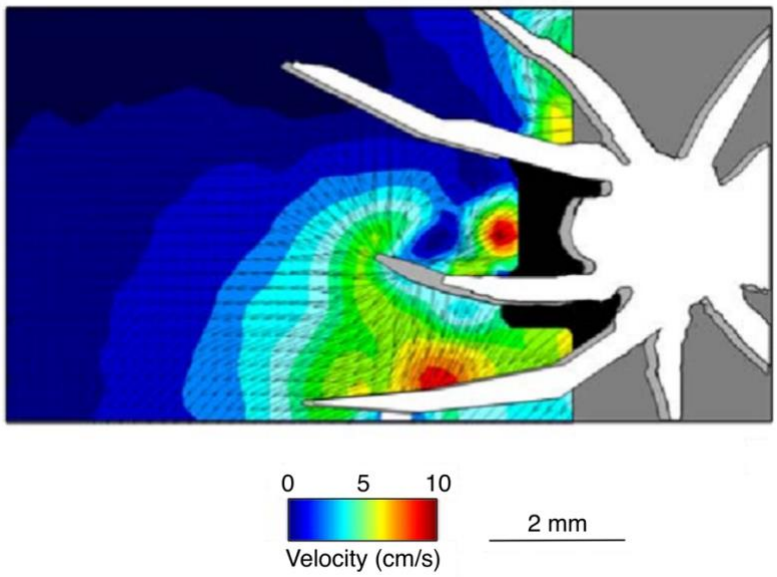

Figure 4.1. Horizontal flow field and close-up view of the flow around a running spider (modified from Casas et al., 2008). An overlay of two images (first image in white, second image in grey) of the moving spider, separated by 500 ms, is shown. The zone of flow velocities above the measurable range is in black.

The detection of a spider elicits an escape response (jumping). However, defense behavior including headstand (sudden raise of the abdomen), stilt stand (tilting of the whole body while the abdomen in raised), and kicking with the hind legs (Figure 2; Gnatzy and Heusslein, 1986), has also been observed in response to approaching *Liris niger*, a hunting wasp that paralyzes crickets to provide food for its brood. This broad array of antipredator behaviors suggests that crickets are capable of encoding not only the velocity and location of the threat but also additional information on its characteristics that triggers stereotyped responses.

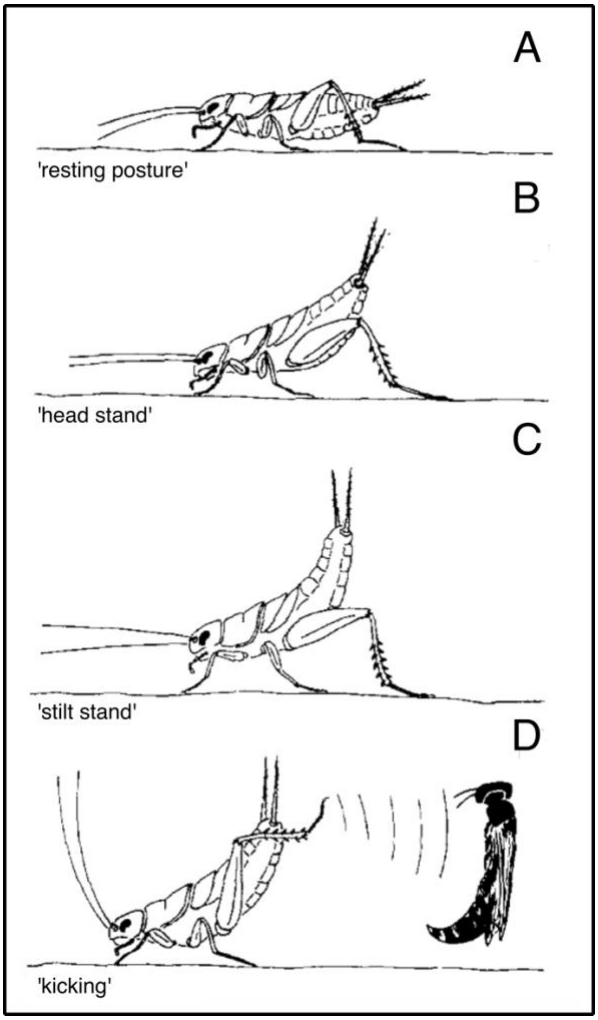

Figure 4.2. Body postures of the cricket *Acheta domesticus* (modified from Gnatzy and Heusslein, 1986). A) resting posture, B-D) defensive reactions to attacks of *Liris niger*.

Since both conspecifics and predators are relatively small, one stimulus feature that may distinguish biologically relevant from irrelevant stimuli is the presence of small-scale stimulus dynamics. I propose that, in addition to participating in the ensemble encoding of bulk-airflow stimulus characteristics, the primary sensory interneurons of the cricket cercal system are capable of operating as feature detectors for small-scale dynamic stimuli such as those produced by approaching predators, competitors or mates (Chapter 3). Such small-scale dynamics have

previously been considered insignificant, and effort has been made when generating laboratory stimuli to ensure that they were not present. My results show that, by limiting the stimuli used to test this system, only a partial understanding of these cells' function has been obtained.

Neurons have beautiful, complex shapes determined by their genetic and developmental programs that can be visualized through histological procedures. But how much can these shapes tell us about the neuron's function? Major aspects of the stimulus-response specificity of these interneurons can be understood from the dendritic anatomy and connectivity with the sensory afferent map. Using multiple extracellular recordings and a special sensory stimulation device, I show that four well-studied interneurons (left and right INs 10-2a and 10-3a) respond with high sensitivity and selectivity to complex dynamic multi-directional features of air currents which have a spatial scale smaller than the physical dimensions of the cerci. The air particle velocity threshold for these features is substantially lower than the threshold for simple unidirectional bulk-flow stimuli used in previous studies. The new tuning surfaces thus show that the cricket cercal system encodes information on the direction and location of moving air and responds to stimuli that vary on spatial scales similar to those of many ecologically relevant predator and conspecific signals. In this sense, these interneurons may be encoding and transmitting information about different aspects of their stimulus environment: they are multiplexing information. These results challenge our understanding of this model system and suggest that directional tuning assumed until now only describes these IN's behavior over a limited subset of stimuli.

References

Casas, J., Steinmann, T., Dangles, O., 2008. The aerodynamic signature of running spiders. PLoS ONE 3, e2116. https://doi.org/10.1371/journal.pone.0002116

Gnatzy, W., Heusslein, R., 1986. Digger wasp against crickets: I. Receptors involved in the antipredator strategies of the prey. Naturwissenschaften 73, 212–215. https://doi.org/10.1007/BF00417728

Mulder-Rosi, J., Cummins, G.I., Miller, J.P., 2010. The cricket cercal system implements delay-line processing. Journal of Neurophysiology 103, 1823–1832. https://doi.org/10.1152/jn.00875.2009

REFERENCES CITED

Aldworth, Z. N., Dimitrov, A. G., Cummins, G. I., Gedeon, T., & Miller, J. P. (2011). Temporal encoding in a nervous system. *PLoS Computational Biology*, *7*(5), e1002041. *PLoS Computational Biology*, *7*(5), e1002041.

Baba, Y., Hirota, K., & Yamaguchi. (1991). Morphology and response properties of wind-sensitive non-giant interneurons in the terminal abdominal ganglion of crickets. *Zoological Science*, *8*, 437–445.

Baba, Y., Hirota, K., Yamaguchi, T., & Shimozawa, T. (1995). Differing afferent connections of spiking and nonspiking wind-sensitive local interneurons in the terminal abdominal ganglion of the cricket Gryllus bimaculatus. *Journal of Comparative Physiology A*, *176*(1). https://doi.org/10.1007/BF00197749

Bacon, J. P., & Murphey, R. K. (1984). Receptive fields of cricket giant interneurones are related to their dendritic structure. *The Journal of Physiology*, *352*(1), 601–623. https://doi.org/10.1113/jphysiol.1984.sp015312

Beckius, G. E., Batra, R., & Oliver, D. L. (1999). Axons from anteroventral cochlear nucleus that terminate in medial superior olive of cat: Observations related to delay lines. *The Journal of Neuroscience*, *19*(8), 3146–3161. https://doi.org/10.1523/JNEUROSCI.19-08-03146.1999

Bennett, M. (1971). Electric organs. In *Fish Physiology* (pp. 347–491). Academic Press.

Bodnar, D. A. (1993). Excitatory influence of wind-sensitive local interneurons on an ascending interneuron in the cricket cercal sensory system. *Journal of Comparative Physiology A*, *172*(5), 641–651. https://doi.org/10.1007/BF00213686

Bodnar, DeanaA., Miller, JohnP., & Jacobs, GwenA. (1991). Anatomy and physiology of identified wind-sensitive local interneurons in the cricket cercal sensory system. *Journal of Comparative Physiology A*, *168*(5), 553–564. https://doi.org/10.1007/BF00215077

Butts, D. A., & Goldman, M. S. (2006). Tuning curves, neuronal variability, and sensory coding. *PLoS Biology*, *4*(4), e92. https://doi.org/10.1371/journal.pbio.0040092

Carr, C. E. (1993). Processing of temporal information in the brain. *Annual Review of Neuroscience*, *16*(1), 223–243. https://doi.org/10.1146/annurev.ne.16.030193.001255

Carr, C. E., & Konishi, M. (1988). Axonal delay lines for time measurement in the owl's brainstem. *Proceedings of the National Academy of Sciences*, *85*(21), 8311–8315. https://doi.org/10.1073/pnas.85.21.8311

Carr, C., Heiligenberg, W., & Rose, G. (1986). A time-comparison circuit in the electric fish midbrain. I. Behavior and physiology. *The Journal of Neuroscience*, *6*(1), 107–119. https://doi.org/10.1523/JNEUROSCI.06-01-00107.1986

Casas, J., & Dangles, O. (2010). Physical Ecology of Fluid Flow Sensing in Arthropods. *Annual Review of Entomology*, *55*(1), 505–520. https://doi.org/10.1146/annurev-ento-112408-085342

Casas, J., & Steinmann, T. (2014). Predator-induced flow disturbances alert prey, from the onset of an attack. *Proceedings of the Royal Society B: Biological Sciences*, *281*(1790), 20141083. https://doi.org/10.1098/rspb.2014.1083

Casas, J., Steinmann, T., & Dangles, O. (2008). The aerodynamic signature of running spiders. *PLoS ONE*, *3*(5), e2116. https://doi.org/10.1371/journal.pone.0002116

Chapman, K. M., & Pankhurst, J. H. (1967). Conduction velocities and their temperature coefficients in sensory verve fibres of cockroach jegs. *Journal of Experimental Biology*, *46*(1), 63–84. https://doi.org/10.1242/jeb.46.1.63

Comer, C., Mara, E., Murphey, K., Getman, M., & Mungy, M. (1994). Multisensory control of escape in the cockroach Periplaneta americana. *Journal of Comparative Physiology A*, *174*, 13–26.

Cummins, B., Gedeon, T., Klapper, I., & Cortez, R. (2007). Interaction between arthropod filiform hairs in a fluid environment. *Journal of Theoretical Biology*, *247*(2), 266–280. https://doi.org/10.1016/j.jtbi.2007.02.003

Cummins, G. I., Crook, S. M., Dimitrov, A. G., Ganje, T., Jacobs, G. A., & Miller, J. P. (2003). Structural and biophysical mechanisms underlying dynamic sensitivity of primary sensory interneurons in the cricket cercal sensory system. *Neurocomputing*, *52–54*, 45–52. https://doi.org/10.1016/S0925-2312(02)00786-5

Dangles, O., Casas, J., & Coolen, I. (2006). Textbook cricket goes to the field: The ecological scene of the neuroethological play. *Journal of Experimental Biology*, *209*(3), 393–398. https://doi.org/10.1242/jeb.02000

Dangles, O., Irschick, D., Chittka, L., & Casas, J. (2009). Variability in sensory ecology: Expanding the bridge between physiology and evolutionary biology. *The Quarterly Review of Biology*, *84*(1), 51–74. https://doi.org/10.1086/596463

Dangles, O., Ory, N., Steinmann, T., Christides, J.-P., & Casas, J. (2006). Spider's attack versus cricket's escape: Velocity modes determine success. *Animal Behaviour*, *72*(3), 603–610. https://doi.org/10.1016/j.anbehav.2005.11.018

Dupuy, F., Steinmann, T., Pierre, D., Christidès, J.-P., Cummins, G., Lazzari, C., Miller, J., & Casas, J. (2012). Responses of cricket cercal interneurons to realistic naturalistic stimuli in the field. *Journal of Experimental Biology*, *215*(14), 2382–2389. https://doi.org/10.1242/jeb.067405

Edwards, J., & Palka, J. (1974). The cerci and abdominal giant fibres of the house cricket, *Acheta domesticus*. I. Anatomy and physiology of normal adults. *Proceedings of the Royal Society of London. Series B. Biological Sciences*, *185*(1078), 83–103. https://doi.org/10.1098/rspb.1974.0007

Gnatzy, W., & Heusslein, R. (1986). Digger wasp against crickets: I. Receptors involved in the antipredator strategies of the prey. *Naturwissenschaften*, *73*(4), 212–215. https://doi.org/10.1007/BF00417728

Gnatzy, W., & Kamper, G. (1990). Digger wasp against crickets. II. An airborne signal produced by a running predator. *Journal of Comparative Physiology A*, *167*(4). https://doi.org/10.1007/BF00190826

Heinzel, H.-G., & Dambach, M. (1987). Travelling air vortex rings as potential communication signals in a cricket. *Journal of Comparative Physiology A*, *160*(1), 79–88. https://doi.org/10.1007/BF00613443

Huang, Y., & Miller, J. (2004). Phased-array processing for spike discrimination. *Journal of Neurophysiology*, *92*, 1944–1957.

Jacobs, G. A., Miller, J. P., & Aldworth, Z. (2008). Computational mechanisms of mechanosensory processing in the cricket. *Journal of Experimental Biology*, *211*(11), 1819–1828. https://doi.org/10.1242/jeb.016402

Jacobs, G. A., & Murphey, R. K. (1987). Segmental origins of the cricket giant interneuron system. *The Journal of Comparative Neurology*, *265*(1), 145–157. https://doi.org/10.1002/cne.902650110

Jacobs, G. A., & Theunissen, F. E. (2000). Extraction of sensory parameters from a neural map by primary sensory interneurons. *The Journal of Neuroscience*, *20*(8), 2934–2943. https://doi.org/10.1523/JNEUROSCI.20-08-02934.2000

Jacobs, G., & Miller, J. (1983). Cellular mechanisms underlying directional sensitivity of an identified sensory interneuron. *Journal of Neuroscience*, *6*, 2298–2311.

Jacobs, G., & Miller, J. (1985). Functional properties of individual neuronal branches isolated in situ by laser photoinactivation. *Science*, *228*(4697), 344–346. https://doi.org/10.1126/science.3983633

Jacobs, G., & Pittendrigh, C. (2002). Predicting emergent properties of neuronal ensembles a database of individual neurons. In *Computational Neuroanatomy* (pp. 151–170). Humana Press.

Jacobs, G., & Theunissen, F. (1996). Functional organization of a neural map in the cricket cercal sensory system. *The Journal of Neuroscience*, *16*(2), 769–784. https://doi.org/10.1523/JNEUROSCI.16-02-00769.1996

Kamper, G., & Dambach, M. (1981). Response of the cercus-to-giant interneuron system in crickets to species-specific song. *Journal of Comparative Physiology ? A*, *141*(3), 311–317. https://doi.org/10.1007/BF00609933

Landolfa, M., & Jacobs, G. (1995). Direction sensitivity of the filiform hair population of the cricket cercal system. *Journal of Comparative Physiology A*, *177*, 759–766.

Magal, C., Dangles, O., Caparroy, P., & Casas, J. (2006). Hair canopy of cricket sensory system tuned to predator signals. *Journal of Theoretical Biology*, *241*(3), 459–466. https://doi.org/10.1016/j.jtbi.2005.12.009

Mellon, D., & Christison-Lagay, K. (2008). A mechanism for neuronal coincidence revealed in the crayfish antennule. *Proceedings of the National Academy of Sciences*, *105*(38), 14626–14631. https://doi.org/10.1073/pnas.0804385105

Miller, J. P., & Jacobs, G. A. (1984). Relationships between neuronal structure and function. *The Journal of Experimental Biology*, *112*, 129–145.

Miller, J. P., Jacobs, G. A., & Theunissen, F. E. (1991). Representation of sensory information in the cricket cercal sensory system. I. Response properties of the primary interneurons. *Journal of Neurophysiology*, *66*(5), 1680–1689. https://doi.org/10.1152/jn.1991.66.5.1680

Miller, J. P., Krueger, S., Heys, J. J., & Gedeon, T. (2011). Quantitative characterization of the filiform mechanosensory hair array on the cricket cercus. *PLoS ONE*, *6*(11), e27873. https://doi.org/10.1371/journal.pone.0027873

Mulder-Rosi, J., Cummins, G. I., & Miller, J. P. (2010). The cricket cercal system implements delay-line processing. *Journal of Neurophysiology*, *103*(4), 1823–1832. https://doi.org/10.1152/jn.00875.2009

Ogawa, H., Baba, Y., & Oka, K. (1996). Dendritic Ca2+ response in cercal sensory interneurons of the cricket Gryllus bimaculatus. *Neuroscience Letters*, *219*(1), 21–24. https://doi.org/10.1016/S0304-3940(96)13162-1

Ogawa, H., Baba, Y., & Oka, K. (1999). Dendritic Ca2+ transient increase evoked by wind stimulus in the cricket giant interneuron. *Neuroscience Letters*, *275*(1), 61–64. https://doi.org/10.1016/S0304-3940(99)00744-2

Ogawa, H., Baba, Y., & Oka, K. (2000). Spike-dependent calcium influx in dendrites of the cricket giant interneuron. *Journal of Neurobiology*, *44*(1), 45–56. https://doi.org/10.1002/1097-4695(200007)44:1<45::AID-NEU5>3.0.CO;2-#

Ogawa, H., Baba, Y., & Oka, K. (2001). Dendritic calcium accumulation regulates wind sensitivity via short-term depression at cercal sensory-to-giant interneuron synapses in the cricket. *Journal of Neurobiology*, *46*(4), 301–313.

Ogawa, H., Baba, Y., & Oka, K. (2002a). Spike-triggered dendritic calcium transients depend on synaptic activity in the cricket giant interneurons. *Journal of Neurobiology*, *50*(3), 234–244. https://doi.org/10.1002/neu.10032

Ogawa, H., Baba, Y., & Oka, K. (2002b). Direction of action potential propagation influences calcium increases in distal dendrites of the cricket giant interneurons. *Journal of Neurobiology*, *53*(1), 44–56. https://doi.org/10.1002/neu.10105

Ogawa, H., Baba, Y., & Oka, K. (2004). Directional sensitivity of dendritic calcium responses to wind stimuli in the cricket giant interneuron. *Neuroscience Letters*, *358*(3), 185–188. https://doi.org/10.1016/j.neulet.2004.01.023

Ogawa, H., Cummins, G. I., Jacobs, G. A., & Miller, J. P. (2006). Visualization of ensemble activity patterns of mechanosensory afferents in the cricket cercal sensory system with calcium imaging. *Journal of Neurobiology*, *66*(3), 293–307. https://doi.org/10.1002/neu.20220

Ogawa, H., Cummins, G. I., Jacobs, G. A., & Oka, K. (2008). Dendritic design implements algorithm for synaptic extraction of sensory information. *Journal of Neuroscience*, *28*(18), 4592–4603. https://doi.org/10.1523/JNEUROSCI.5354-07.2008

O'Shea, M., & Adams, M. E. (1981). Pentapeptide (proctolin) associated with an identified neuron. *Science*, *213*(4507), 567–569. https://doi.org/10.1126/science.6113690

Palka, J., Levine, R., & Schubiger, M. (1977). The cercus-to-giant interneuron system of cricket. *Journal of Comparative Physiology A*, *119*, 267–283.

Paydar, S., Doan, C. A., & Jacobs, G. A. (1999). Neural mapping of direction and frequency in the cricket cercal sensory system. *The Journal of Neuroscience*, *19*(5), 1771–1781. https://doi.org/10.1523/JNEUROSCI.19-05-01771.1999

Pfeiffer, K., & French, A. S. (2015). Naturalistic stimulation changes the dynamic response of action potential encoding in a mechanoreceptor. *Frontiers in Physiology*, *6*. https://doi.org/10.3389/fphys.2015.00303

Pumphrey, R., & Rawdon-Smith, A. (1937). Synaptic transmission of nervous impulses through the last abdominal ganglion of the cockroach. *Proceedings of the Royal Society of London. Series B - Biological Sciences*, *122*(826), 106–118. https://doi.org/10.1098/rspb.1937.0013

Rall, W. (1964). Theoretical significance of dendritic trees of neuronal input-output relations. In *Neural Theory and Modeling* (pp. 73–97). Stanford University Press.

Saitoh, I., & Suga, N. (1995). Long delay lines for ranging are created by inhibition in the inferior colliculus of the mustached bat. *Journal of Neurophysiology*, *74*(1), 1–11. https://doi.org/10.1152/jn.1995.74.1.1

Salinas, E., & Abbott, L. F. (1994). Vector reconstruction from firing rates. *Journal of Computational Neuroscience*, *1*(1–2), 89–107. https://doi.org/10.1007/BF00962720

Schnupp, J. W. H., & Carr, C. E. (2009). On hearing with more than one ear: Lessons from evolution. *Nature Neuroscience*, *12*(6), 692–697. https://doi.org/10.1038/nn.2325

Shimozawa, T., & Kanou, T. (1984). The aerodynamics and sensory physiology of range fractionation in the cereal filiform sensilla of the cricket Gryllus bimaculatus. *Journal of Comparative Physiology A*, *155*, 495–505.

Steinmann, T., & Casas, J. (2017). The morphological heterogeneity of cricket flow-sensing hairs conveys the complex flow signature of predator attacks. *Journal of The Royal Society Interface*, *14*(131), 20170324. https://doi.org/10.1098/rsif.2017.0324

Sugihara, I., Lang, E. J., & Llinás, R. (1993). Uniform olivocerebellar conduction time underlies Purkinje cell complex spike synchronicity in the rat cerebellum. *The Journal of Physiology*, *470*(1), 243–271. https://doi.org/10.1113/jphysiol.1993.sp019857

Tauber, E., & Camhi, J. (1995). The wind-evoked escape behavior of the cricket Gryllus bimaculatus: Integration of behavioral elements. *The Journal of Experimental Biology*, *198*(Pt 9), 1895–1907.

Theunissen, F. E., & Miller, J. P. (1991). Representation of sensory information in the cricket cercal sensory system. II. Information theoretic calculation of system accuracy and optimal tuning-curve widths of four primary interneurons. *Journal of Neurophysiology*, *66*(5), 1690–1703. https://doi.org/10.1152/jn.1991.66.5.1690

Theunissen, F., Roddey, J. C., Stufflebeam, S., Clague, H., & Miller, J. P. (1996). Information theoretic analysis of dynamical encoding by four identified primary sensory interneurons in the cricket cercal system. *Journal of Neurophysiology*, *75*(4), 1345–1364. https://doi.org/10.1152/jn.1996.75.4.1345

Troyer, T. W., Levin, J. E., & Jacobs, G. A. (1994). Construction and analysis of a database representing a neural map. *Microscopy Research and Technique*, *29*(5), 329–343. https://doi.org/10.1002/jemt.1070290502

Young, J. (1939). Fused neurons and synaptic contacts in the giant nerve fibres of cephalopods. *Philosophical Transactions of the Royal Society of London. Series B, Biological Sciences*, *229*(564), 465–503. https://doi.org/10.1098/rstb.1939.0003